

INTERNATIONAL ENERGY AGENCY

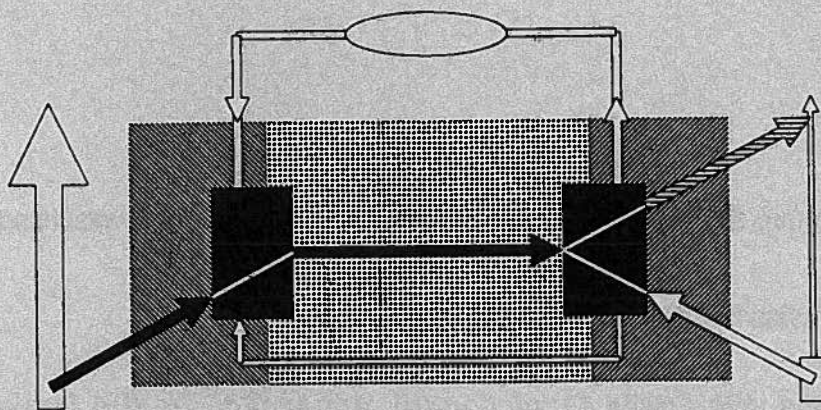
Programme of R, D & D on Advanced Fuel Cells

Annex II : Modelling & Evaluation of Advanced SOFC

EF Nr. 192853

Final report

SOFC STACK DESIGN TOOL



Swiss Federal Office of Energy, Operating Agent Task II

Berne, November 1992.

Editor : Léo Dubal, Swiss Federal Office of Energy, CH - 3003 Berne (Switzerland)

Copyright : Swiss Federal Office of Energy

In accordance with article 11 section (h), Annex II of the IEA Implementing Agreement for a Programme of R,D&D on Advanced Fuel Cells, reproduction in full or in part is authorized only for Denmark, Germany, Italy, Japan, The Netherlands, Norway, Switzerland, and United Kingdom. It is mandatory to cite the report title in the following form:

"STACK DESIGN TOOL, an International Energy Agency SOFC Task Report, Berne, November 1992".

PREFACE:

THE IEA PROGRAMME OF R, D & D ON ADVANCED FUEL CELLS

International Energy Agency

The International Energy Agency was formed in November 1974 to establish cooperation among a number of industrialized countries in the vital area of energy policy. It is an autonomous body within the framework of the Organization of Economic Cooperation and Development (OECD). Twenty-two countries are presently members, with the Commission of the European Communities also participating in the work of the IEA under a special arrangement.

Programme of R,D&D on Advanced Fuel Cells

The IEA Implementing Agreement for a Programme of R,D&D on Advanced Fuel Cells was established in April 1990 and comprised initially two annexes. One dealt with the analysis of the Balance-of-Plant of Molten Carbonate Fuel Cells and the other with the Modelling and Evaluation of Advanced Solid Oxide Fuel Cells. Five new annexes are in preparation. There are now ten signatories to the agreement: Denmark (DEA), Germany (KFA-Jülich on behalf of BMFT), Italy (ENEA), Japan (NEDO), the Netherlands (NOVEM), Norway (NCSIR), Spain (Hidroeléctrica Espanola), Sweden (NEA), Switzerland (OFEN), United Kingdom (DOE).

Annex II: Modelling and Evaluation of Advanced Solid Oxide Fuel Cells

The collaborative effort was scheduled for an initial two year term of Annex II, with Switzerland acting as Operating Agent. The targeted objective was to advance natural gas-fuelled solid oxide fuel cells technologies through:

- i) the numerical modelling of innovative concepts which have the potential for low-cost mass production and higher conversion efficiency; the establishment of the necessary experimental data base and the model validation;*
- ii) the elaboration of recommended practices for SOFC products evaluation and their application to available SOFCs in order to assist the development taking place in industry, strengthen confidence and prevent confusion in the market.*

The original signatories were Italy, Japan, the Netherlands, Norway, and Switzerland. They have been joined by the United Kingdom, Denmark and Germany.

The task-sharing work has been divided into seven *activities*, each with an appointed *activity leader*:

- i) Stack Design Tool (Norway)*
- ii) Micromodelling (Switzerland)*
- iii) SOFC Data (Denmark)*
- iv) Recommended Practices for Electrochemical Evaluation (United Kingdom)*
- v) Recommended Practices for Thermomechanical Evaluation (Italy)*
- vi) Recommended Practices for Powder Characterisation (The Netherlands)*
- vii) Recommended Practices for Stack Evaluation (Japan)*

Augustin McEvoy, from the Federal Institute of Technology, in Lausanne, acted as Operating Agent on behalf of the Swiss Federal Office of Energy. Continuation of Annex II is presently being discussed.

Final report
STACK DESIGN TOOL

Activity leader : Norway

<u>CONTENTS</u>	page
1. Executive summary	1
2. Mathematical modelling of Monolithic SOFC Elisabetta Arato and Paolo Costa (Italy)	6
3. 3-D Numerical Model for SOFC Stacks Monica Østenstad (Norway)	18
4. SOFC Two Dimensional "Unit Cell" Modelling James R. Ferguson (Switzerland)	31
5. Numerical Simulation of solid oxide fuel cells at the cell and stack level. J.M. Fiard, R. Herbin (Switzerland)	50
Appendix: Benchmark case definition	69

1. Executive summary

During the IEA SOFC Workshop at Hertenstein in Switzerland in June 1990, it was recognized that it would be appropriate to divide the modelling activity within the Annex into two separate activities. These activities were the Micromodelling activity and the Stack Modelling activity, which was later called the Stack Design Tool.

This is a natural division. While the main objective of the Micromodelling activity has been to be able to build better electrodes through a better understanding and quantitative modelling of the fundamental microscopic processes, the stack models takes the electrochemical performance of a given PEN (Positive air electrode/Electrolyte/Negative fuel Electrode) as an input to the calculations. The purpose of stack modelling is to be able to predict stack performance as a function of stack design and stack operating conditions in order to test out design alternatives and optimize the stack design.

II. Stack modelling

Stack models should be able to predict how overall performance is influenced by the important design parameters. One important set of design parameters are the channel dimensions, the thickness of the electrodes etc. In order to resolve this geometry a very finely spaced numerical mesh is needed. If this mesh is extended to cover the whole stack, we will get a problem which is too large to be solved within reasonable time limits.

One answer to this problem is to do modelling on two separate levels. On the lowest level detailed calculations are done on a domain covering only one unit cell of the stack. The computational results from this model can be used to produce, through homogenization techniques, "average" material parameters for the unit cell. These "average" material parameters can then be used as input for stack models that can simulate the whole stack. The detailed unit cell geometry is only seen by the stack model through the value of the "average" material parameters.

Three levels of modelling have been included in the Stack Design Tool activity. This is the detailed modelling of a unit cell, homogenized cell models covering one plate of the stack and a three dimensional model which can be used to simulate a whole stack of plates. Models can be extended further to include the manifolds, the unit where the stack is enclosed and finally auxiliary equipment like heat exchangers, external reformers etc. Including auxiliary equipment brings us into the area of system modelling. This has not been included in the activity. Also only very simple modelling of manifolds and the heat exchange between stack and the enclosing unit have been considered.

Design models are usually stationary models. They compute a solution assuming that all the temporal transients in the system has died out. Dynamic models on the other hand can compute the temporal development of the solution. Dynamic modelling is necessary in order to provide a stack model that can be used to give guidelines for startup and shutdown procedures, to investigate stability and multiplicity of solutions, to investigate control strategies and to simulate the effect of load level variations. From a modellers point of view, a dynamic model is an extension of the stationary model, where the transient heating of the stack and possibly the dynamics of fuel and gas transport is included. The Italian participants at ISTIC (University of Genova) has developed a dynamic cell modell for the simulation of transient behaviour in SOFC cells (Chapter 2).

III. Task activities

The most active parties in the Stack Design Tool activity has been Italy, Norway, Switzerland and to some degree the Netherlands.

As a result of the Hertenstein workshop a collaboration was started between the Norwegian and the Swiss parties. The aim of this collaboration has been to develop numerical models both at the unit cell level and at the stack level, and to provide the means for using results from the unit cell simulation as input data to the stack modelling level. The Swiss party has been working mainly on the unit cell modelling and on how the unit cell results can be included as input data to a stack model (see chapter 4 and 5), while the main emphasis for the Norwegian party has been on stack modelling (see Chapter 3).

The Italian group at ISTIC (University of Genova) have been working on a dynamic model for the simulation of the transient behaviour of SOFC cells due to variations in the electrical power. Investigations of control strategies has been made using the same operating constraints as those required for a PAFC industrial plant. The TNO (The Netherlands) has done some modelling, mainly concentrating on pressure drop calculations in the channels in order to assess the minimum dimensions of the gas channels. Some investigations has also been done on the effect of numerical diffusion in regions with large temperature gradients.

Model validation

At the Workshop in Oslo (August 1992) the need for model validation and verification was extensively discussed. At this stage experimental data which can be used to validate stacks, is scarce. Instead it was decided to define a standard bench mark case for stack models so that models can be tested against each other.

A flat plate crossflow design was selected as the standard case. This bench mark case consists of a form describing the input parameters in general terms and a form for reporting the results (Appendix). The test has been run on the Norwegian and the Italian stack models.

IV. Review and commentary on received contributions

Mathematical modelling of Monolithic SOFC

Elisabetta Arato and Paolo Costa (Italy)

This contribution is a summary of the work which have been done by the authors on the stack and cell modelling and simulation. The twodimensional steady state model developed by the authors is presented together with a comparative study of the cross-, co- and counterflow configurations. The results show the best performance for the counterflow configuration. The importance of the heat exchange between the stack and the surroundings for performance is also illustrated by this study.

The steady state model has been used as a starting point for a dynamic model which describes the transient behaviour of the cell system under different control procedures. The model used for these studies are essentially the same as the static model. The only transient phenomena which is necessary to include in the model, is the thermal relaxation. The characteristic time scale for the other transient phenomena in the cell is much shorter, and they can essentially be assumed to be in equilibrium.

Various control procedures for the stack can be simulated by controlling model inputs with a control strategy based on model outputs, and the temporal behaviour of the stack under closed loop control can be studied.

In addition, work relating to the flow distribution in manifolds and the effect on the stack performance due to an uneven feeding of reactants to the plates in the stack, is presented.

3-D Numerical Model for SOFC Stacks

Monica Østenstad (Norway)

This paper gives a short description of the stack model which has been developed in Norway as part of the IEA cooperation. The model is based on homogenized electrical and thermal conductivities from a unit cell model. The computational domain of the model can be the whole stack or a part of the stack, for instance one plate with interconnect. The model supports simple manifolding, so that partly spent fuel and air can be resirculated.

The model solves for the electrical potential distribution, the temperature distribution in the fuel, the air and the interconnect, and the species concentrations in the fuel and air channels. The potential computation is based on the three dimensional charge balance equation. The temperature computations are based on the energy balances, including convective and conductive heat transfer, chemical and electrochemical reaction heat generation and heat generated due to ohmic and overpotential losses. The computation of the species concentrations in the fuel and air channels is based on the mass balance equation, including the electrochemical reaction and the reforming and shift reaction.

In the report the model is used for studying the potential benefits of a metallic interconnector and to study internal reforming in the stack. Due to the increased thermal conductivity of a metal interconnector, the stack temperature distribution will be more even. This means that the stack performance will be better. For the internal reforming case a configuration is studied where internal reforming takes place in separate plates. The reformed fuel is then manifolded back through ordinary fuel channels in counterflow to the reformer channels. The heat needed for the reforming reaction can then be supplied by the heat generated by the electrochemical reaction, and the temperature gradients within the cell can be drastically reduced.

SOFC Two Dimensional "Unit Cell" Modelling

James R. Ferguson (Switzerland)

This work is about the detailed modelling of a flat plate co- or counterflow unit cell. The computational domain is two dimensional and consists of the interconnect, the anode, the electrolyte and the cathode. The temperature and the molar concentrations in the fuel and air channels are boundary conditions to the model. The solution of the governing equations in the model gives the temperature distribution and the electrical current distribution throughout the unit cell. In the anode and the cathode the molar concentrations of hydrogen and oxygen respectively, are also obtained.

The model is based on heat conduction in the unit cell, diffusive mass transport in the anode and the cathode, and ohmic currents in the whole unit cell. The temperature and the mass transport equations are coupled to the temperature and the molar concentrations in the fuel and air channels through the appropriate boundary conditions. At the anode/electrolyte and the cathode/electrolyte boundaries the potential is discontinuous due to the Nernst potential and the overpotentials. This is awkward to treat mathematically. Therefore the stream function for the current distribution is used instead of the electric potential in order to compute the current distribution. This transforms away the problem with the discontinuities. Only the total Nernst potential and overpotentials needs to be known in this formulation and there is no need to decompose it into two half potentials.

The model can be used for studying potential losses in the unit cell, both ohmic losses and losses due to slow diffusion of the reactive species. The losses can be studied as a function of unit cell geometry and material parameters. The model could therefore be a help for improving the cell design. The model can also be used to obtain homogenized electrical and thermal conductivities, where the effect of the geometry, the inplane conduction and the overpotentials are included, for use in models describing the operations of complete stacks.

Numerical Simulation of solid oxide fuel cells at the cell and stack level.

Raphaele Herbin, Jean-Michel Fiard (Switzerland)

This work presents a two dimensional model of a co- or counterflow planar unit cell and results obtained by numerical simulation. The model which have been implemented is essentially the one described in the preceeding work. The temperature and the electrical current distribution in the unit cell is computed together with the molar concentrations of hydrogen and oxygen in the anode and cathode respectively. Input to the model is the geometry of the unit cell, material properties (thermal and electrical conductivities and diffusion coefficients), temperatures and compositions in the channels and the average current density through the cell. A series of numerical results are presented in the report including temperature and current distributions for typical situations. The results concerning the effect of electrode diffusion seem to confirm that diffusion overvoltages is not a limiting factor under normal operating conditions.

The model presented here can be used to generate input data for stack models using ideas from homogenization theory, through the computation of equivalent thermal and electrical conductivities.

Oslo, November 1992

Activity leader "Stack Design Tool"

Terje Sira

Institutt for energiteknikk, Norway

MATHEMATICAL MODELLING OF MONOLITHIC SOFC

Elisabetta Arato and Paolo Costa

ISTIC - University of Genoa - GENOA (ITALY)

Introduction

In order to help in the rational design and the effective utilization of commercial fuel cells a number of reliable simulation tools have been developed.

As in the study of chemical heterogeneous reactors, two different levels of investigation can be considered in the analysis of fuel cells. At a microscopic level the intrinsic electrodic kinetics and transport phenomena of mass and charge inside porous electrodes can be studied [6, 7, 9]; on this scale heat transfer phenomena are not limiting, so that local isothermicity can be assumed. Then, at a macroscopic level, the mass and heat transport in the gaseous streams and the heat transfer through the solid phases and between solids and gases can be considered.

So, a single cell can be simulated using a two-dimensional monolithic model [8-10, 17, 19], while a stack of cells needs a three-dimensional description which takes into account some symmetry conditions. The mathematical models describing the steady state behaviour of monolithic SOFC devices with external reforming for different gas flow geometries and the transient response under a control system are presented. A comparison between cross, counter and co-current flows is considered and the related distributions of temperature and electrical current are discussed.

In addition, some questions arising from flow distribution in industrial practice are also presented. A non-homogeneous distribution of reactants in stack manifolds could cause e.m.f. differences between cells at the top and the bottom of the module. Explanation in terms of inertial effects can suggest the way of improving the manifold design.

The steady-state model of a cell

A mathematical steady-state simulation of a monolithic fuel cell with external reforming, under the assumption of a uniform cell voltage, has been developed [2, 8].

The cell is crossed by cathodic and anodic orthogonal porous gas channels with a cross section of about 1 mm². The cathodic channels bring an oxygen rich gas, while the anodic ones bring fuel: the global chemical reaction leads to the formation of two moles of vapour at the anode for each one of oxygen consumed. The Reynolds number of a channel is typically less than 10 whereas the Péclet number is greater or much greater than 20: as a consequence the mass and heat balances for the gaseous flows result in a plug-flow description [8, 10, 13, 14, 16, 18]. In addition, the discrete channeling is described as a continuous one in terms of a specific rate per unit length.

So, with reference to anodic and cathodic reaction

$$\sum_i k_{ij} A_i + k_{ej} = 0 \quad j=1,2 \quad k_{e1} + k_{e2} = 0 \quad (1)$$

mass and heat balances are written in the form:

$$\partial y_j / \partial z_j = r \quad j=1,2 \quad (2)$$

$$G_{ij} = G_{ij0} + k_{ij} y_j; \quad x_{ij} = G_{ij} / \sum_i G_{ij} \quad j=1,2, \quad i=1,2,\dots,c \quad (3)$$

$$(G_j \sum_i x_{ij} C_{pi}) \partial T_j / \partial z_j = r \sum_i k_{ij} C_{pi} (T - T_j) + \alpha_j a_j (T - T_j) \quad j=1,2 \quad (4)$$

with the boundary conditions:

$$z_j = 0 \quad y_j = 0 \quad j=1,2 \quad (5)$$

$$z_j=0 \quad T_j=T_{j0} \quad j=1,2 \quad (6)$$

where subscript i indicates the component, $j=1,2$ indicates the cathodic and the anodic flows respectively, z_j ($j=1,2$) being the axial coordinate of each flow. These in general may differ from the orthogonal coordinates of the cell which will be indicated as z_3 and z_4 . The reaction rate r , expressed by means of local kinetic models [6, 7] or, lacking more detailed information, by a simplified one [1], and the generation rates r_{ij} are connected with each other and to the current density by means of stoichiometric links:

$$r_{ij} = k_{ij} r \quad j=k_{e2} F r = -k_{e1} F r \quad (7)$$

So, the local energetic balance of the cell, under the assumption of uniform temperature along the cell thickness, can be written as:

$$\partial^2 T / \partial z_3^2 + \partial^2 T / \partial z_4^2 = -Q_d / \lambda \delta + \sum_j \alpha_j (T - T_j) / \lambda \delta \quad (8)$$

with the boundary conditions:

$$z_j=0 \quad T / z_j = \alpha_a (T - T_a) / \lambda \quad j = 3,4 \quad (9)$$

$$z_j=Z_j \quad T / z_j = -\alpha_a (T - T_a) / \lambda \quad j = 3,4 \quad (10)$$

In equation (8) the heat conductivity is the result of averaging on the composite structure of the cell and the heat sources corresponding to dissipations are

$$Q_d = (-\Delta H - k_{e2} V F) r \quad (11)$$

The cell is described by a grid of finite elements and the mass and heat balances equation for the gaseous streams are directly solved once the temperature of the solid is known. In the static cell description [8, 9] the Fourier problem with distributed heat sources is integrated by a relaxation method, which recognizes and follows the trend of natural temporal evolution of solid temperature, introducing fictitious times.

The code of the model has been developed in a Fortran 77 software package which runs on a 486 50 MHz clock. Input data are geometrical characteristics of the cell, inlet flow conditions, external load and required electrical power; as results, local temperature of the solid and gases, composition of anodic and cathodic flow, electrical current and cell voltage are computed.

Figure 1 reports the results of the steady-state simulation, in terms of solid temperature (1a) and electrical current density (1b) fields, when the benchmark input data shown in table I are utilized and gas and material properties are drawn from [5]. In table II the mean values of output variables are indicated.

Flow geometry effects

Cross-flow geometry is the simplest geometry that can be easily achieved in fuel cell devices [13, 15, 17], but different constructing solutions can be considered to obtain a good cell performance with high electrical efficiency and a quite uniform distribution of operating variables [2, 14, 19].

In order to obtain a significant comparison between different geometries, standard input data have been used for all the tests (see table III). Adiabatic and non-adiabatic conditions have been assumed. Among the results, temperature and electrical current fields have been examined. The temperature of the solid generally shows a maximum which occurs at the outlet section of the cathodic flow. Under non-adiabatic conditions this maximum is shifted into the inner part of the cell, its position depending on heat exchange through the external surface. The trend of the electrical current is similar to the solid temperature trend, but current maxima also strongly depend on the concentration fields of gaseous reagents, especially on the oxygen one. This influence in particular can be detected in the counter flow case where the current maximum is located in the inner position with respect to the temperature maximum due to a higher oxygen concentration. Besides, in a cross-flow cell maxima and minima of the electrochemical driving force occur at opposite edges instead of at opposite sides of the cell as in the case of counter and co-flow.

**STEADY-STATE SIMULATION OF AN ADIABATIC SOFC CELL:
BENCHMARK INPUT DATA**

Gas channel dimensions	0.1X0.1 cm
Cell dimensions	10X10 cm
External resistance	2.7 ohm cm ²
Pressure	1 atm
Inlet anodic temperature	1000 K
Inlet cathodic temperature	1000 K
Anodic gaseous flow	97% H ₂ +3% H ₂ O
Cathodic gaseous flow	20% O ₂ +80% N ₂
Anodic flowrate	2.04 10 ⁻⁴ mole s ⁻¹
Cathodic flowrate	2.04 10 ⁻⁸ mole s ⁻¹

Table I: Cross-flow planar SOFC simulation with external reforming: benchmark input data.

BENCHMARK TEST: MEAN VALUES OF OUTPUT VARIABLES

Solid temperature (K)	1122
Current density (mA cm ⁻²)	311.2
Anode temperature at outlet (K)	1074.5
Cathode temperature at outlet (K)	1201.4
H ₂ utilization at outlet (-)	0.815
O ₂ utilization at outlet (-)	0.198
Solid temperature - anode temperature at outlet (K)	-0.012
Solid temperature - cathode temperature at outlet (K)	+1.023
Cell voltage (volt)	0.84

Table II: Cross-flow planar SOFC simulation with external reforming: mean values of output variables.

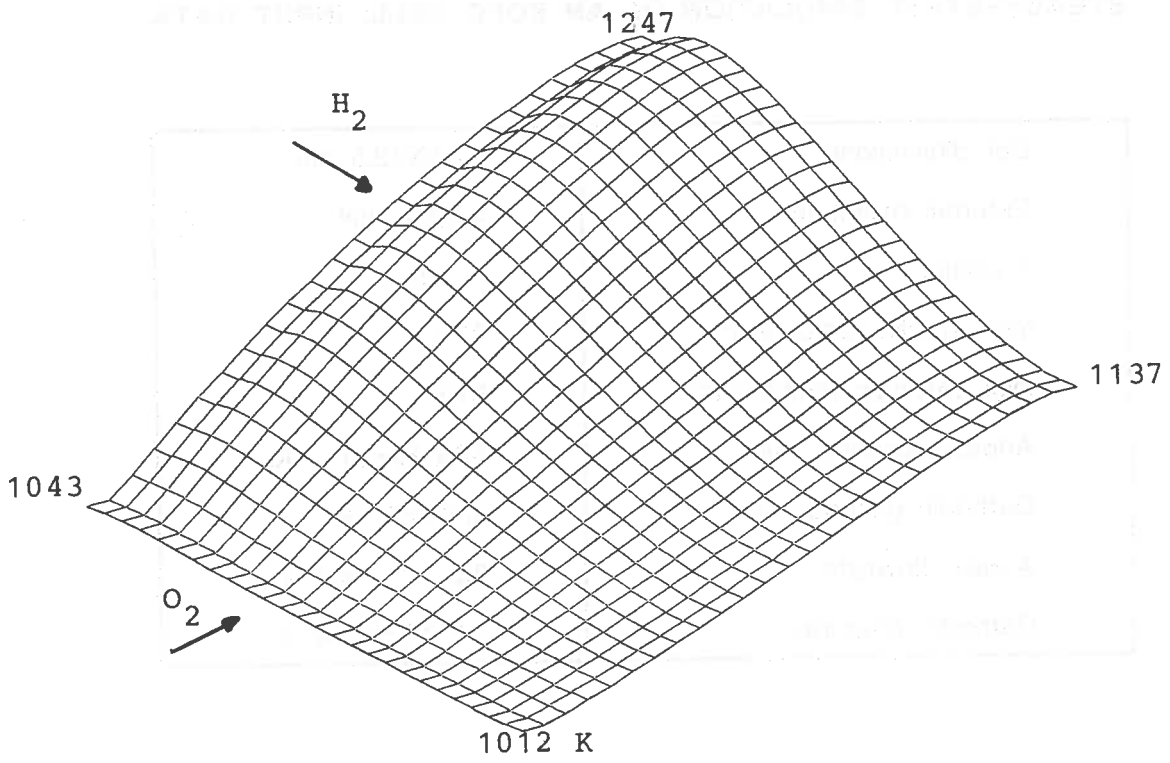


Figure 1a

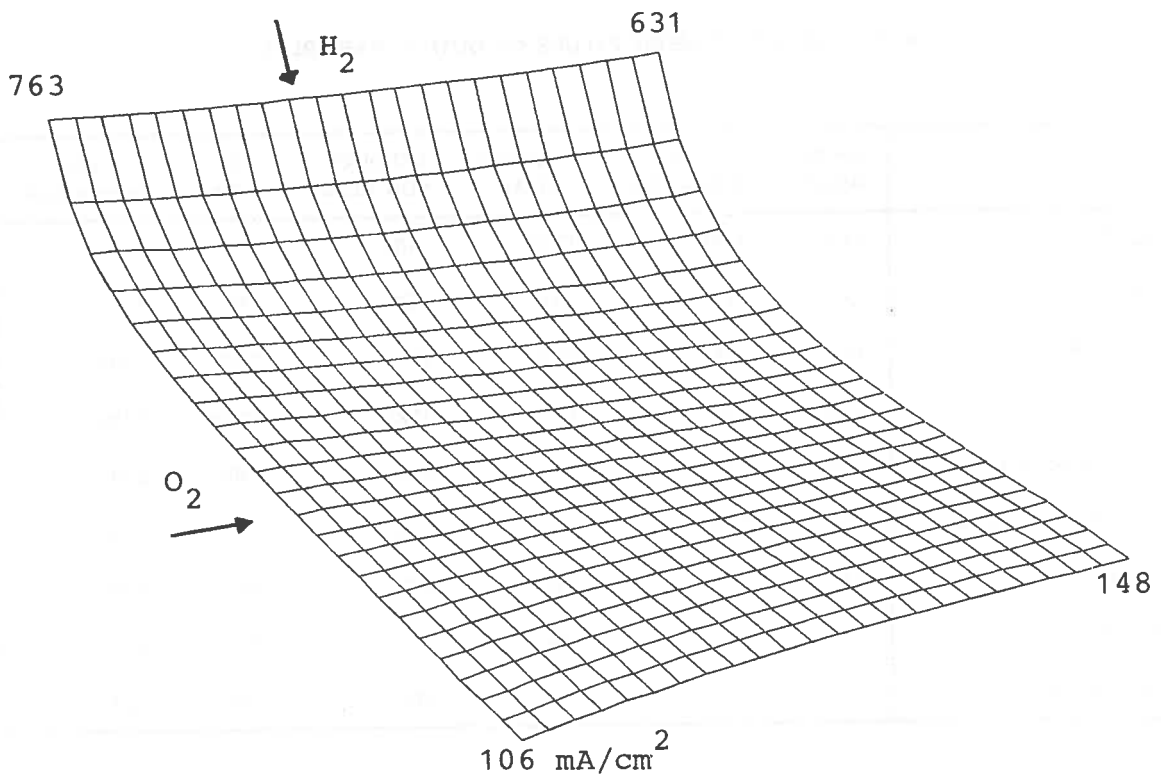


Figure 1b

Figure 1: Two-dimensional solid temperature (K) (1a) and current density (mA/cm²) (1b) profiles corresponding to the adiabatic run of table I. Corner values are indicated.

STEADY-STATE SIMULATION OF AN SOFC CELL: INPUT DATA

Cell dimensions	12.5X12.5 cm
External resistance	4 ohm cm ²
Pressure	1 atm
Inlet anodic temperature	873 K
Inlet cathodic temperature	973 K
Anodic gaseous flow	80% H ₂ +20% CO ₂
Cathodic gaseous flow	ambient air
Anodic flowrate	2.2 10 ⁻⁴ mole s ⁻¹
Cathodic flowrate	1.5 10 ⁻³ mole s ⁻¹

Table III: Standard input data for the steady-state simulation of monolithic SOFC cells.

SOFC SIMULATION: MEAN VALUES OF OUTPUT VARIABLES

	CROSS ADIAB.	CROSS NON ADIAB.	COUNTER ADIAB.	COUNTER NON ADIAB.	CO ADIAB.	CO NON ADIAB.
T _{cell} (K)	1136	1098	1212	1136	1141	1082
j (mA cm ⁻²)	151	147	181	152	152	145
T _{anode out} (K)	1170	1094	1030	977	1283	1183
T _{cathode out} (K)	1263	1197	1340	1225	1283	1183
H ₂ utilization at outlet (-)	0.68	0.68	0.73	0.68	0.68	0.65
O ₂ utilization at outlet (-)	0.20	0.19	0.21	0.20	0.20	0.19
V (volt)	0.61	0.59	0.85	0.61	0.61	0.58
j*V (mW cm ⁻²)	92	87	104	93	92	84
-Q _d (mW cm ⁻²)	104	103	104	104	104	103

Table IV: Output variables for different flow geometries of SOFC cells under adiabatic and non-adiabatic conditions.

In table IV a summary of the averaged values of main output variables for the above geometries, obtained for maximum dissipative conditions, is reported. As was expected, under the same inlet conditions, the counter flow cell performs better than co-current and cross flow ones showing highest electrical power and global cell efficiency [19]: apart from trivial constructing aspects there are no particular reasons to prefer the last flow geometry to the counter-current geometry.

Previous investigation has demonstrated that lumped cross-flow reactors may allow a number of stable-steady states, some of them being exclusively due to the lumped character of the simulated system. However, checks on fuel cell simulation have shown that multiplicity does not appear under usual working conditions, probably due to a lower sensitivity of electrochemical reaction to temperature and compositions than to overvoltages. and because the inlet flows are sufficiently preheated. Such findings agree with other results on the simulation of monolithic reactors [10-12]: multiplicity can occur in counter-flow systems and only exceptionally in cross-flow systems.

Operating conditions

A fuel cell can work in a suitable and safe way if some defined operating conditions are achieved [3]. In particular, we have already simulated the transients, due to variations of the required electrical power, of a 1 MW PAFC stack (Milan, Ansaldo Company) and then we have used a similar approach to study the dynamic behaviour of an SOFC cell.

Allowable limits for the 1 MW PAFC plant are reported in the sequence.

The electrochemical module of a fuel cell stack can support load changes in the range 30%-100% of the nominal power and a limit to the rate of this variation equal to 10% of the nominal power in a minute is imposed; in addition, the requested performances must be restricted within the following operating limits of the cell components:

- to reduce the corrosive process within the cell the electrical voltage supplied by the cell must be limited to between a minimum and a maximum value. For example this range can be approximately 0.6-0.8 volt;
- in PAFC modules a refrigerant plate is placed every five or seven cells; the coolant removes the heat produced by the electrochemical reaction, which is proportional to the generated electrical current. Hence the maximum current density allowed for the cell is fixed by the maximum capacity of the refrigerant plates. In the current density - cell voltage plane the above limits define an allowable zone where the cell works without damage;
- another limit is represented by the amount of hydrogen within the cell. In particular if the hydrogen concentration is lower than the cell capacity an oxidation reaction of the graphite of the electrodes may occur, causing serious damage to the cell. Hence for each operating condition the cell must work under hydrogen excess. Typically, the maximum output utilization factor for the hydrogen (defined as hydrogen consumed over hydrogen supplied) should not exceed 80%.

The control system

In commercial devices undesirable operating conditions must be avoided by utilizing an efficient control system which constrains the cells to perform within the allowable limits.

The control of the electrical power of a fuel cell plant can be accomplished by two main control loops: the control loop of the inverter system and of oxygen fed to the cell [3].

In the first loop the required power (or the cell voltage) is compared to the real power (or the fixed voltage) and according to this difference the impedance of inverter, that is the external load, is modified. So, the electrical current and the cell voltage will change according to the static characteristic of the cell. This control system ensures also that the voltage of the cell lies in the allowable range. The second control loop allows the overcoming of limits imposed by the requirement of a constant oxygen concentration behaviour by means of two different steps that regulate both the flowrate and the concentration of oxygen supplied to the cell. The cathodic flowrate recirculation, i.e. the oxygen concentration in the cell, is regulated according to the difference between the electrical power generated and the required one, while the fresh air flowrate is regulated so as to achieve the set point of the produced electrical current. The latter is proportional to the quantity of oxygen consumed in the cell.

Notice that in the industrial plant the above regulation loops occur simultaneously.

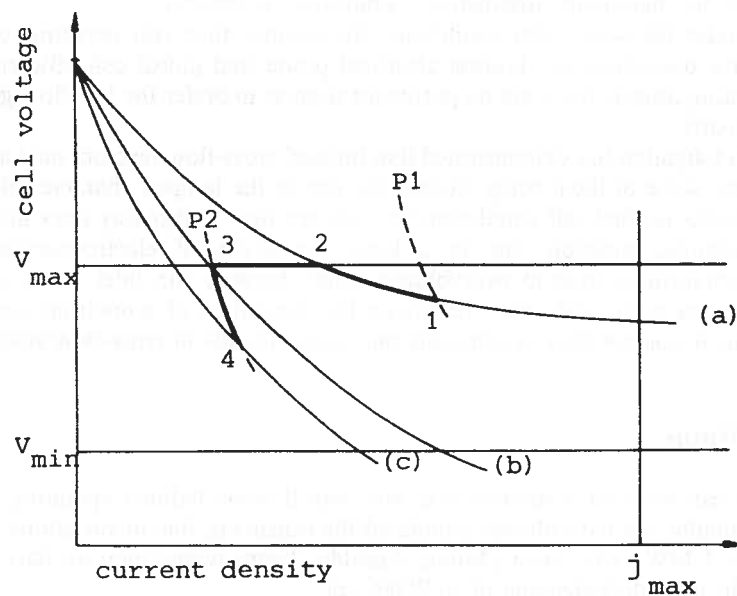


Figure 2: Sketch of the transient behaviour of a fuel cell module due to a power reduction from P1 to P2: cell voltage versus current density. The allowable operating zone for the cell is indicated.

In the light of the above considerations a picture of the transient behaviour due to a load reduction can be given in figure 2, where the I-V characteristics of the cell [(a), (b), (c)] and some curves corresponding to constant power (P1, P2) are reported. Starting from the point 1, corresponding to an electrical power P1 and fixed feeding conditions, a power reduction until P2 is required. The cell responds immediately to this request and the point representing the real state of the system moves along the (a) curve until the point 2. At the same point the cell voltage has reached the maximum value and so the inverter control prevents a further decrease of cell power. Meanwhile the oxygen concentration is reduced by recirculating the cathodic flow. This is equivalent to modifying the static characteristic of the cell from the (a) curve to the (b) curve. The representative point of the state of the cell moves from 2 to 3 that lies on the curve corresponding to the required power P2.

Since it is not safe to have the cell working for a long time at the maximum voltage, a further decrease of oxygen concentration can cause the variation of the static characteristic from the (b) curve to the (c) curve. Then the point representing the final state of the cell moves from 3 to 4 at the same power P2.

The controlled dynamic model

The static model has been utilized as a starting one to derive a dynamic tool [1, 3] which describes the transient behaviour of the cell system under different control procedures. Restoring a full physical meaning for the time variable is one of the main problems in converting the static model into a dynamic one. This approach is equivalent to assuming thermal relaxation on the cell plane as the controlling transient phenomenon. Indeed, the thermal relaxation time, which can be directly evaluated from the equivalent conductivity of the cell, results in by far the largest among all the characteristic times of the other elementary phenomena involved.

All the local times are sufficiently short (only a few seconds) with respect to the thermal relaxation time (some hours in a 1 MW PAFC); so our "thermal" model can give a good description to relatively slow transients. In the light of these considerations, the assumed hypotheses and the model equations already presented for the static description of a fuel cell are directly available for the description of transients due to a load variation.

In the dynamic simulation model the output variables are linked to input variables through a suitable regulation procedure in order to describe the transient response of the cell.

A set point value for output variables is assigned. Some choices are straightforward: for example the fuel utilization can be fixed equal to 0.8. This value can be steadily reached by varying the gaseous flowrate within a characteristic time of a few seconds.

For other variables the problem is more difficult and different control procedures are possible. In particular the cell voltage could be varied within a given range (between the minimum and the maximum value). However, a set point value of the cell voltage close to the maximum value allowable for the cell is suggested by energy considerations.

To reach the fixed voltage and the required power level two choices are available. A first procedure (A) is to control the cell voltage by load changes and the electrical power by cathodic oxygen composition variations; the second procedure (B) is the opposite: the electrical power control is obtained through external load variations and the voltage control through oxidant composition variations.

An example of the transient behaviour of SOFC in terms of cell power density and oxygen concentration in the inlet cathodic flow is reported in figure 3a. The plot refers to an (A) type control procedure, where the electrical power variation is obtained by recirculating the oxygen. The dotted curve corresponds to a decrease of cell power from P1 to P2 and then an increase to P3. The same simulation is described in figure 3b where the cell power density is given as a function of the reduced time.

The characteristics of two possible choices are under investigation, but, comparing the results of different procedures, some considerations can already be drawn:

- the control of the output utilization factor is fast and stable in both cases;
- by using the (B) type controls the cell tends to work at a voltage higher than the maximum value, while the (A) type control systems force the cell to work at a voltage lower than the limit one. The second control procedure seems more satisfactory;
- in addition, whenever two electrical variables are linked -i.e. if the cell voltage is controlled by load changes, as in the (A) type controls- the characteristic control times are very short and the cell works at the maximum voltage during the transient behaviour.

The last remark is less important when a limit on power variation rate is imposed. In fact, if the control system is too fast and the limiting rate of electrical power variation is exceeded, some critical transient behaviours of the cell may occur, in particular when an electrical power increase is required. On the contrary, when a limit of variation of electrical power is imposed, the external load change must occur gradually, so that it can be balanced by the cathodic flowrate increasing; in this case all output variables lie within allowable ranges.

As previously shown, the electrical power control can be achieved also by the regulation of the oxygen concentration supplied to the cell. Severe recirculation is necessary, in particular, when very low power is requested or in correspondence to stand-by conditions; in these cases some important differences in the cell behaviour with respect to the case of nominal operating conditions can be encountered. In figure 4 the simulated electrical current density fields in a counter flow SOFC operating in standard conditions (see table II) and at low oxygen concentration are reported. The latter situation corresponds to a P2 type steady state of figure 3, where a decrease of electrical power is obtained by recirculating the cathodic flow. At low oxygen concentration the trend of solid temperature and electrical current fields are opposite: the maximum of temperature occurs as usual at the outlet section of the oxygen flow, while the maximum of current moves at the oxygen inlet (figure 4b), where the highest oxygen concentration occurs.

Flow distribution

In commercial fuel cell modules e.m.f. differences between cells at the top and the bottom of the stack, probably caused by a non-homogeneous distribution of reactants, have often been regretted. In particular, a bad distribution of anodic flow in the feeding manifold can be explained in terms of inertial effects rather than in terms of hydrogen buoyancy, as some producers assume. By integrating momentum and mass balances over the whole feeding manifold, the gap between the flowrate at the bottom (corresponding to the inlet of fresh total flowrate) and the top of the stack, compared to the mean flowrate, can be computed [4]. Buoyancy effects appear negligible compared to inertial ones. Moreover, inertial anodic effects are more important than cathodic ones and act in the opposite direction to them. More precisely in a 1 MW PAFC stack anodic effects are about ten times greater than cathodic ones and they favour the top of the stack, while in a commercial SOFC stack inertial effects at anode are estimated equal to one and a half times cathodic ones and they favour the bottom of the stack. Therefore the cells located at the top in a PAFC module or at the bottom in an SOFC one are fed on more hydrogen and supply higher electrical tension.

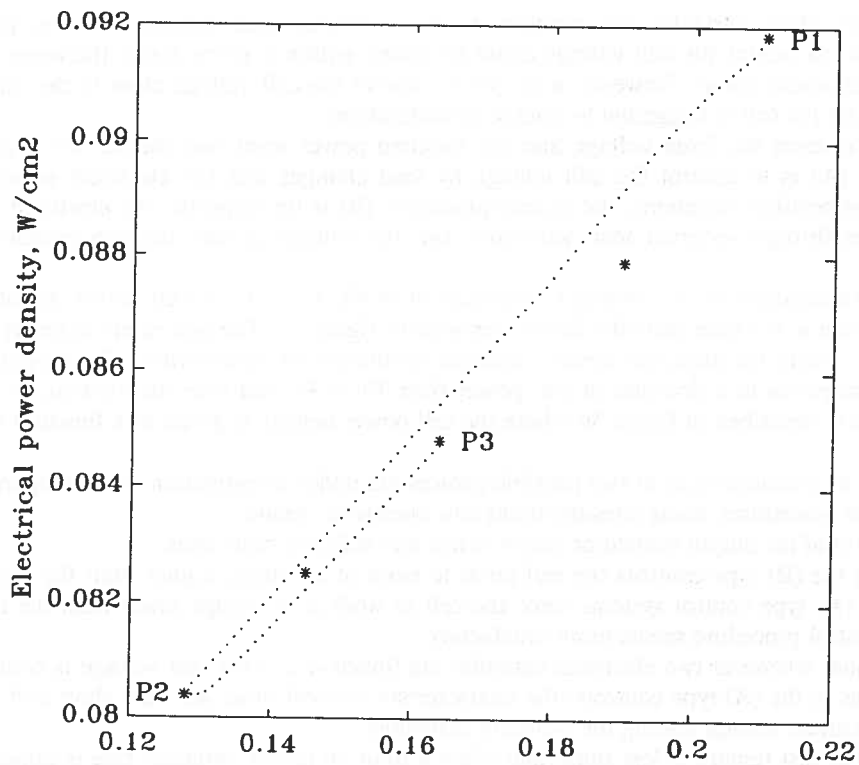


Figure 3a: Oxygen molar fraction in inlet cathodic flow

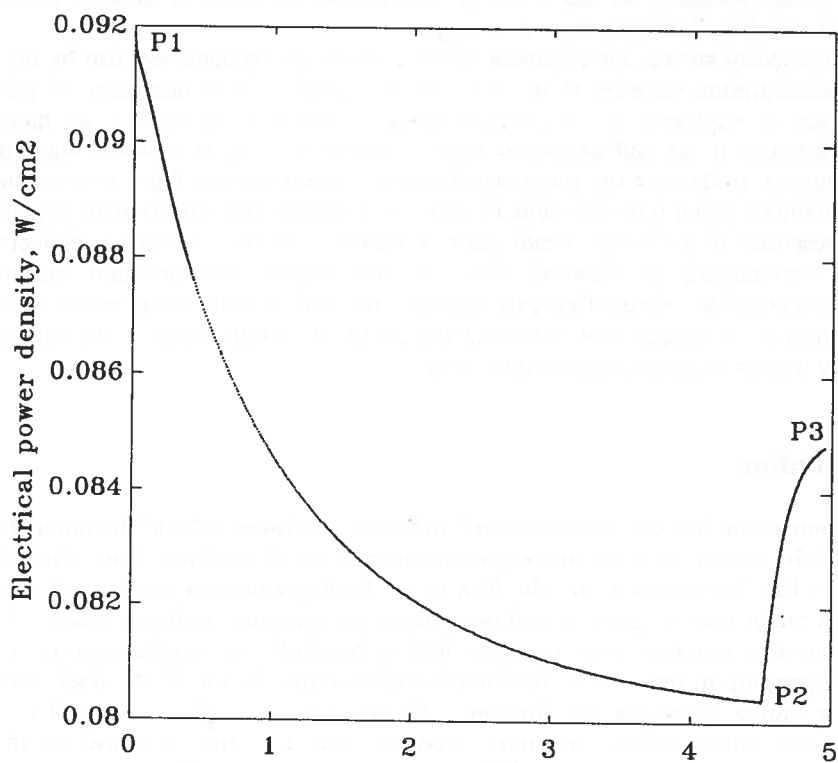


Figure 3b: Reduced time

Figure 3: Transient response of a cross-flow SOFC corresponding to power variation from P1 to P2 and from P2 to P3.

3a: Cell power density versus oxygen concentration. Asterisks indicate steady states. 3b: Cell power density versus reduced time.

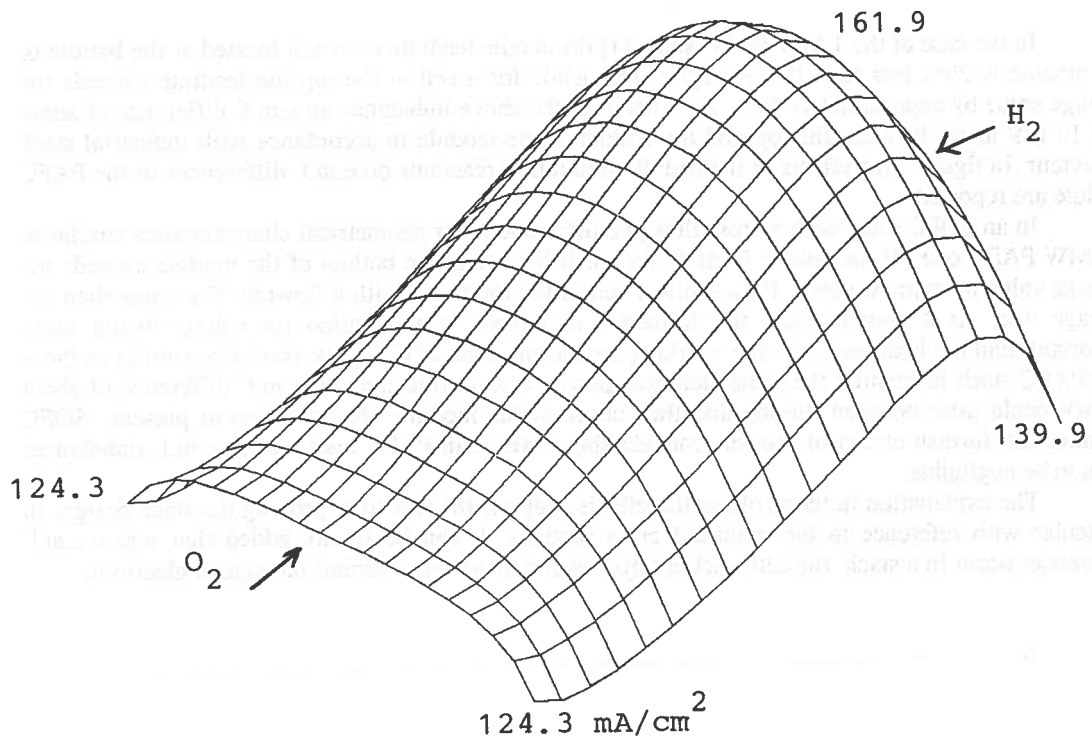


Figure 4a

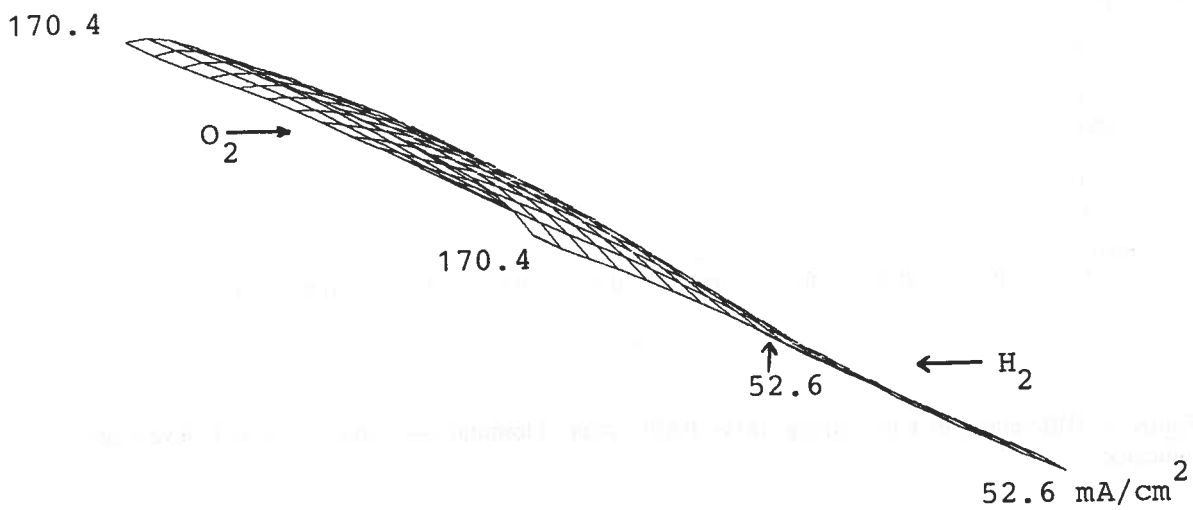


Figure 4b

Figure 4: Counter-flow SOFC cell under non-adiabatic conditions: electrical current density (mA/cm^2) field in standard run (see table III) (4a) and corresponding to very low oxygen concentration ($x_{\text{oxygen}}=0.04$) in the inlet cathodic flow with oxygen and hydrogen utilization factors equal to 0.79 (4b).

In the case of the 1 MW PAFC stack [4] the anodic feedrate for a cell located at the bottom of the module is 20% less than the average value, while for a cell at the top the feedrate exceeds the average value by approximately 10%. As a result of the above imbalance an e.m.f. difference of about 5 to 10 mV arises between the top and the bottom of the module in accordance with industrial stack behaviour. In figure 5 the effects of the bad distribution of reactants on e.m.f. differences in the PAFC module are reported.

In an SOFC stack with a cross flow geometry and other geometrical characteristics similar to a 1 MW PAFC one [4] the anodic feedrate for a cell located at the bottom of the module exceeds the average value by approximately 10%, while a cell at the top is fed with a flowrate 5% lower than the average one. As a consequence, the influence of oxygen concentration on voltage being more important than the hydrogen one, the working conditions of an SOFC stack should be similar to those of a PAFC stack furnishing the same electrical power: also in this case, an e.m.f. difference of about 10 mV could arise between the top and the bottom of the module. Nevertheless at present SOFC modules can furnish electrical power considerably lower than PAFC ones and so e.m.f. imbalances seem to be negligible.

The explanation in terms of inertial effects suggests the way to improving the stack design, in particular with reference to the manifold cross sections. It can be finally added that when e.m.f. differences occur in a stack the cells lacking hydrogen may undergo serious damage at electrodes.

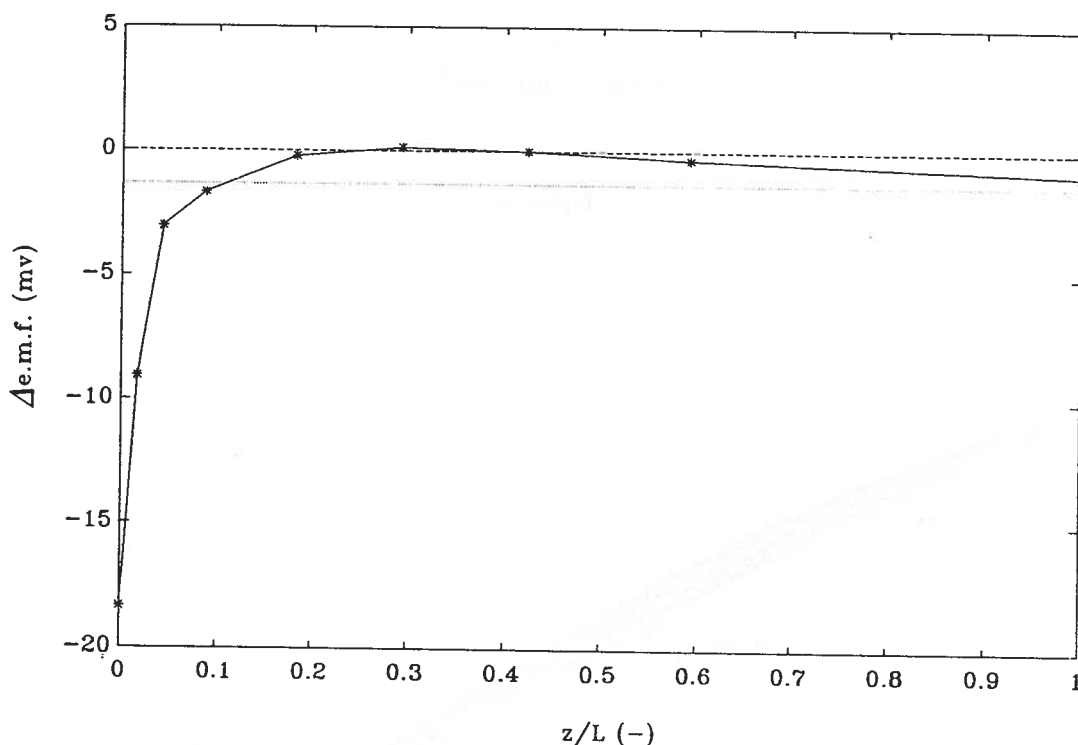


Figure 5: Differences of e.m.f. along 1MW PAFC stack. Nominal (---) and (...) e.m.f. levels are indicated.

References

1. E. Arato, P. Costa, Proc. of 'Second International Symposium on Solid Oxide Fuel Cells' (Athens, Greece, July 1991) 273.
2. E. Arato, O. Paladino, B. Marcenaro, P. Costa, Proc. of 'The International Fuel Cell Conference' (Tokyo, Japan, February 1992), 51.
3. E. Arato, P. Costa, 'Dynamic simulation of fuel cell devices', submitted for publication to *Chem. and Biochem. Eng. Q.*

4. E. Arato, P. Costa, 'Effects of flow distribution in fuel cell stacks', submitted for publication to *Chem. and Biochem. Eng. Q.*
5. U.G. Bossel, *Facts and Figures*, an IEA SOFC Tak Report, Berne, April 1992.
6. P. Costa, E. Arato, B. Canepa, *Chem. and Biochem. Eng. Q.*, **3**, 1989, 111.
7. P. Costa, E. Arato, *Chem. and Biochem. Eng. Q.*, **4**, 1990, 9.
8. P. Costa, E. Arato, L. Maga, O. Paladino, *Chem. and Biochem. Eng. Q.*, **5**, 1991, 43.
9. P. Costa, E. Arato, B. Canepa, *Quaderni dell'Ingegnere Chimico Italiano*, **8-9** of 'La chimica e l'industria', 1991, Q46.
10. P.G. Debenedetti, C.G. Vayenas, *Chem. Eng. Sci.*, **38**, 1983, 1817.
11. T.F. Degnan, Wei J., *AIChEJ*, **25**, 1979, 338.
12. T.F. Degnan, Wei J., *AIChEJ*, **26**, 1980, 60.
13. E. Erdle, J. Groß, H.G. Müller, W.J.C. Müller, Proc. of 'Second International Symposium on Solid Oxide Fuel Cells' (Athens, Greece, July 1991) 265.
14. J. Ferguson, Proc. of 'Second International Symposium on Solid Oxide Fuel Cells' (Athens, Greece, July 1991) 305.
15. J.N. Michaels, C.G. Vayenas, L.L. Hegedus, *J. Electr. Soc.*, **133**, 1986, 522.
16. R. Selman, R. Herbin, M. Fluck, R. Gruber, Proc. of 'IEA SOFC Workshop' (Hertenstein, Switzerland, June 1990), 7.
17. C.G. Vayenas, P.G. Debenedetti, I. Yentekakis, L.L. Hegedus, *Ind. Eng. Chem. Fund.*, **24**, 1985, 316.
18. T.L. Wolf, G. Wilemski, *J. Electr. Soc.*, **130**, 1983, p.48.
19. I.V. Yentekakis, S. Neophytides, S. Seimanides, C.G. Vayenas, Proc. of 'Second International Symposium on Solid Oxide Fuel Cells' (Athens, Greece, July 1991) 281.

Notation

- a = heat transfer area per unit cell area [-];
 A = component
 C_p = molar heat capacity [J/mole K];
 F = Faraday constant [A s/mole];
 G = molar flowrate per unit length [mole/m s];
 j = current density [A/m²];
 k = stoichiometric coefficient [-];
 L = stack height [m];
 P = electrical power [J/s];
 Q = heat flux [J/m² s];
 r = reaction rate for unit cell area [mole/m² s];
 T = absolute temperature [K];
 V = cell voltage [J/A s];
 x = molar fraction [-];
 y = degree of advancement of reaction [mole/m s];
 z = geometrical coordinate [m];
 ΔH = enthalpy of reaction [J/mole];

Greeks

- α = heat transfer coefficient [J/m² s K];
 δ = cell thickness [m];
 λ = heat conductivity of cell [J/m s K];

Indexes

- a = atmospheric
 c = component
 d = dissipated
 e = electron
 i = component
 j = flow
 \max = maximum
 \min = minimum
 0 = inlet

3-D NUMERICAL MODEL FOR SOFC STACKS

Monica Østenstad

Norway

1 Functional Description

A three dimensional computer model for simulation of the thermal, electrical and electrochemical behaviour of an SOFC stack has been developed at IFE (Institutt for energiteknikk in Norway). The first version of the model calculates steady state operation, and it has been applied to flat plate unit cell geometries.

The model can simulate stack operation with methane as well as hydrogen or reformed natural gas as fuel. In the case of methane the model can simulate either internal or integrated reforming, with non-equilibrium integration of the reforming reaction.

The three dimensional character of the model makes it possible to perform realistic calculations of the temperature field in a stack which is in thermal contact with the environment. Another interesting application in 3D is integrated reforming.

2 Chemical Reactions

The chemical reactions which are included in the model are shown on figure 1. Additional reactions may however easily be included in future versions of the model, or some of the reactions which are already included may be disabled. As yet we have not investigated the coking problem, and in any case we do not plan to do any modelling of coking, but only to find out if conditions favouring it may arise.

In the applications for which we have used the model until now we have assumed that:

- Direct oxidation of methane may be disregarded
- The shift reaction goes to equilibrium instantaneously
- The oxidation of CO may be disregarded

- The back-reaction of reforming may be ignored
- The electrochemical reactions take place at electrode/electrolyte interface
- The shift- and reforming reactions take place in fuel channel

The last two assumptions are used in setting up the differential equations for the heat balance. As reaction rate for the shift reaction we use:

$$\bullet \tau_{shift} = K \cdot (k_{eq} \cdot p_{CO} \cdot p_{H_2O} - p_{CO_2} \cdot p_{H_2})$$

here k_{eq} is the equilibrium constant for the shift reaction. If we choose the constant K to be very large we ensure that we always reach the equilibrium concentrations of the reactants and products.

As reaction rate for the reforming reaction we have used /1/:

$$\bullet \tau_{CH_4} = K_0 \cdot e^{-E/RT} \cdot p_{CH_4} \cdot p_{H_2O}^{-1.25}$$

This reaction rate is in units of $mol/(s \cdot g_{catalyst})$ and it only takes into consideration the forward reaction of methane reforming.

At this point I would like to mention that the model is made completely flexible in the sense that the present reaction rates may be exchanged by other functions if they are proven to be better.

3 Mathematical formulation

Figure 2 shows the partial differential equations of the model. The variables of the equations are:

- The oxygen flux in the air flow, l
- The fuel component flux vector, \vec{K}
- The temperature of the air flow, T_a
- The temperature of the fuel flow, T_f
- The temperature of the solid, T_s
- The electrical potential, Φ

The physical entities λ , σ and α are homogenized material constants. The model reads these as functions of temperature from tables. At present the values for σ are produced by a very simple unit cell model made at IFE, which takes into account the influence of geometry and overpotentials. The values used for the λ and α are estimated analytically /2/.

As figure 2 shows the model have to solve a set of two elliptic equations and four transport equations. We have discretized the equations by finite volume methods, and we have used an upstream approximation on the transport equations and a finite difference approximation on the elliptic equations.

The set of discretized equations is solved by iterations on three levels. The outer iteration loop is an iteration between the charge balance and the transport equations. The charge balance equation is solved by a method of preconditioned conjugated gradients. The transport equations and the equation for heat balance in the solid are solved by iteration on the non-linearities and on the heat conduction.

4 Case Studies

We have made three case studies:

1. Crossflow geometry , Hydrogen as fuel, Ceramic interconnect material
2. Crossflow geometry , Hydrogen as fuel, Metallic interconnect material
3. Integrated reforming, Coflow geometry , Methane as fuel

In the first case all changes occur in the x-y plane as described in figure 3. This plane is 10 by 10 cm. Fuel is input in the positive x-direction and air in the positive y-direction. The temperature of both inlet flows are 850 K. There is a potential difference in the z-direction. In the second case the inlet temperatures are 775 K, otherwise the boundary conditions of the two cases are identical. In case 1 we get an average fuel utilization of 0.85, and in case 2 we get 0.88. Figure 4 shows the temperature distribution in the solid for the two cases. We note that the temperature ranges from 923 to 1213 K in the case of ceramic interconnect material, and from 1032 to 1117 K in the case of metallic interconnect material. In other words, the spread in temperature is much less in the case of metallic interconnect material. What effect this has on the current density distribution is shown on figure 5. In the case of ceramic interconnect the crossplane current density ranges from 431 to 4827 A/m^2 . But in the case of metallic interconnect it ranges from 2085 to 3838 A/m^2 . This means that the crossplane current density is more uniform in the case of metallic interconnect material, and this gives fewer losses.

In the third case we have simulated a stack which is build as alternate zones of electrochemical plates and reformer channels. This case is described on figure 6. We have assumed that there are symmetry planes in the middle of each zone, in which case we get all the information we need by considering the area between two such planes. We also have assumed that a reasonable design would be that each electrochemical zone consist of five plates and each reformer zone of one reformer channel. This gives the dimensions shown on the figure. Methane is fed

to the reformer zone in the positive x-direction. At the reformer outlet the fuel gases are collected in a manifold, resirculated and fed into the electrochemical zone in coflow with air.

In this case we get a fuel utilization of 0.89, and a temperature profile as shown on figure 7. It is obvious that some of the heat developed in the electrochemical zone is conducted to the reformer zone where it is needed to drive the reforming reaction. This is the purpose of the integrated design. We also note that the difference between highest and lowest temperature is only 53 K in this case.

Finally I have written a summary table for the three cases (figure 8). If we compare cases 1 and 2 (ceramic vs. metallic interconnect material) we find that the difference between maximum and minimum temperature, the maximum temperature gradient and the spread in utilization is much less in the case of metallic interconnect. The same conclusion is found for the comparison between cases 1 and 3. The integrated reforming case lowers temperature gradients and the spread in temperature and utilization.

As a final conclusion I would like to say that both the use of a metallic interconnect material (if possible in practice) and the use of integrated reforming seems like promising concepts. From the three cases we have run it seems as these designs offer considerable advantages to that of case 1, by virtue of smaller variations in temperature and fuel utilization and thereby fewer losses.

5 References

- [1] Ivar Dahl, "SOFC Reforming Chemistry", presented at IEA workshop on mathematical modelling on SOFC, Hertenstein june 24 to 29 1990.
- [2] A. Solheim, "Case-studie. Forslag til dimensjoner og anslaatte data" , August 1991.

6 Nomenclature

6.1 Roman symbols

Φ	electrical potential (V)
l	oxygen flux density ($mol/(m^2s)$)
\vec{K}	fuel flux density vector ($mol/(m^2s)$)
T_s	solid temperature (K)
T_a	air temperature (K)
T_f	fuel temperature (K)
j	current density ($A \cdot m^{-2}$)

j_z	current density crossplane ($A \cdot m^{-2}$)
N_a	molar flux density of air ($mole \cdot s^{-1}m^{-2}$)
N_f	molar flux density of fuel ($mole \cdot s^{-1}m^{-2}$)
U_N	the Nernst potential (V)
\vec{r}	array of reaction rates ($mole \cdot s^{-1}m^2$)
ΔH	enthalpy change by chemical reaction ($J \cdot mol^{-1}$)
p	pressure (Pa)
C_p	specific heat capacity ($J \cdot mol^{-1}K^{-1}$)
A	matrix of stoichiometric coefficients (-)
F	Faradays constant

6.2 Greek symbols

σ	electrical conductivity ($\Omega^{-1}m^{-1}$)
α	coefficient of heat transfer ($W \cdot m^{-3}K^{-1}$)
λ	thermal conductivity ($W \cdot K^{-1}m^{-1}$)
ξ	number of electrochemical plates per meter in z-direction (m^{-1})

1. Oxidation of H_2 :



2. Oxidation of CO :



3. Direct oxydation of methane :



4. An endothermic reforming reaction which takes place at the surface of nickel :



5. The shift reaction :



6. Methane dissoociation :



7. The Boudouard reaction :



$$\frac{\partial l(z_a)}{\partial z_a} = -\frac{j_z}{4F} \cdot \xi_{EC} \quad (1)$$

$$N_a C_p^a \frac{\partial T_a}{\partial z_a} = \alpha_s^a (T_s - T_a) \quad (2)$$

$$\frac{\partial K_\gamma}{\partial z_f} = A_\gamma^T \cdot \vec{r} \cdot \xi_F \quad (3)$$

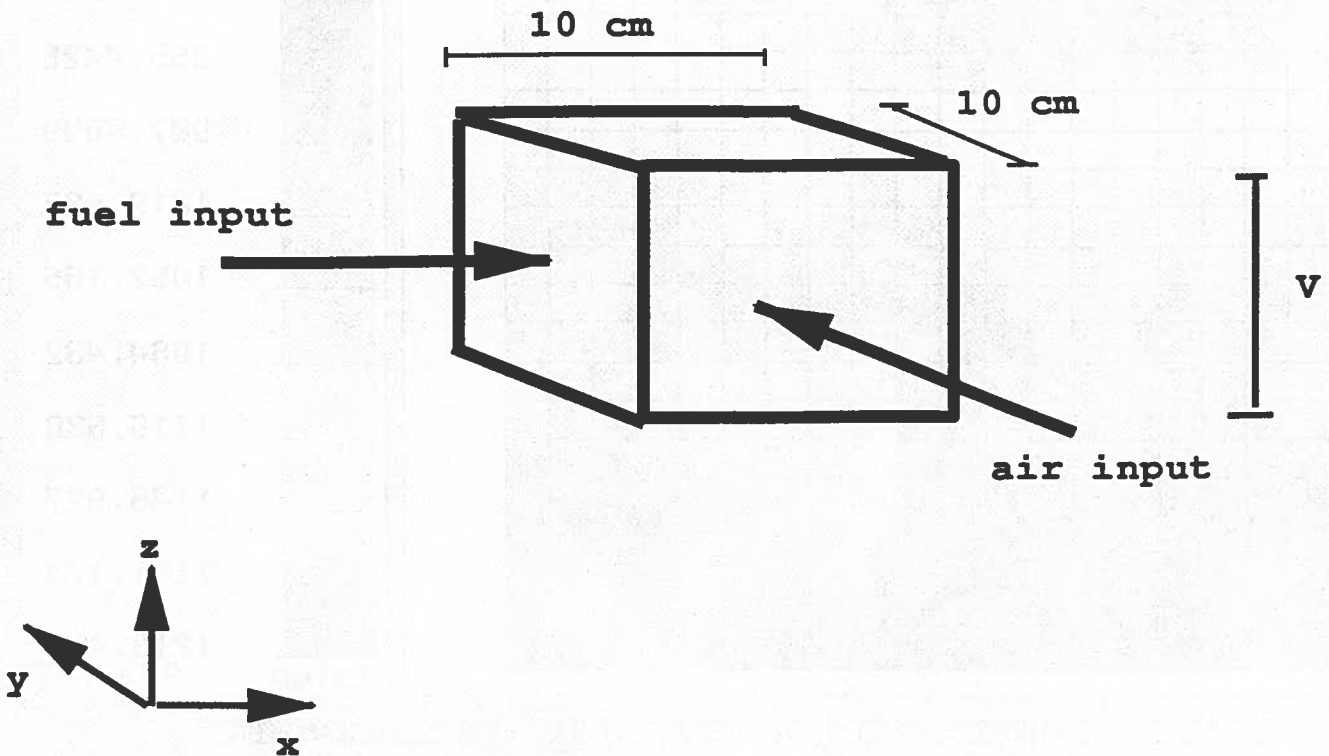
$$N_f C_p^f \frac{\partial T_f}{\partial z_f} = \alpha_s^f (T_s - T_f) - \sum_{\beta=n_{EC}+1}^{n_{max}} \Delta H_\beta \cdot r_\beta \cdot \xi_F \quad (4)$$

$$-\nabla \lambda \nabla T_s = \alpha_s^a (T_a - T_s) + \alpha_s^f (T_f - T_s) - \sum_{\beta=1}^{n_{EC}} \Delta H_\beta \cdot r_\beta \cdot \xi_F - \vec{j} \cdot \nabla \Phi \quad (5)$$

$$\frac{\partial}{\partial x} \sigma_x \frac{\partial \Phi}{\partial x} + \frac{\partial}{\partial y} \sigma_y \frac{\partial \Phi}{\partial y} + \frac{\partial}{\partial z} \sigma_z \left(\frac{\partial \Phi}{\partial z} - U_N \cdot \xi_{EC} \right) = 0 \quad (6)$$

FIGURE 2

FIGURE 3
DESCRIPTION OF CASE 1

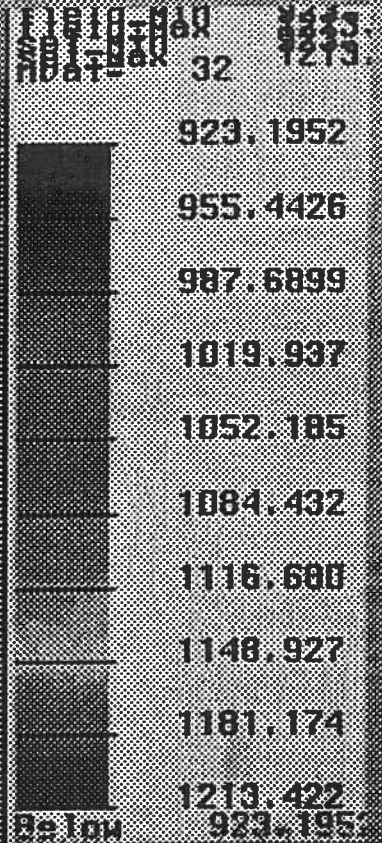
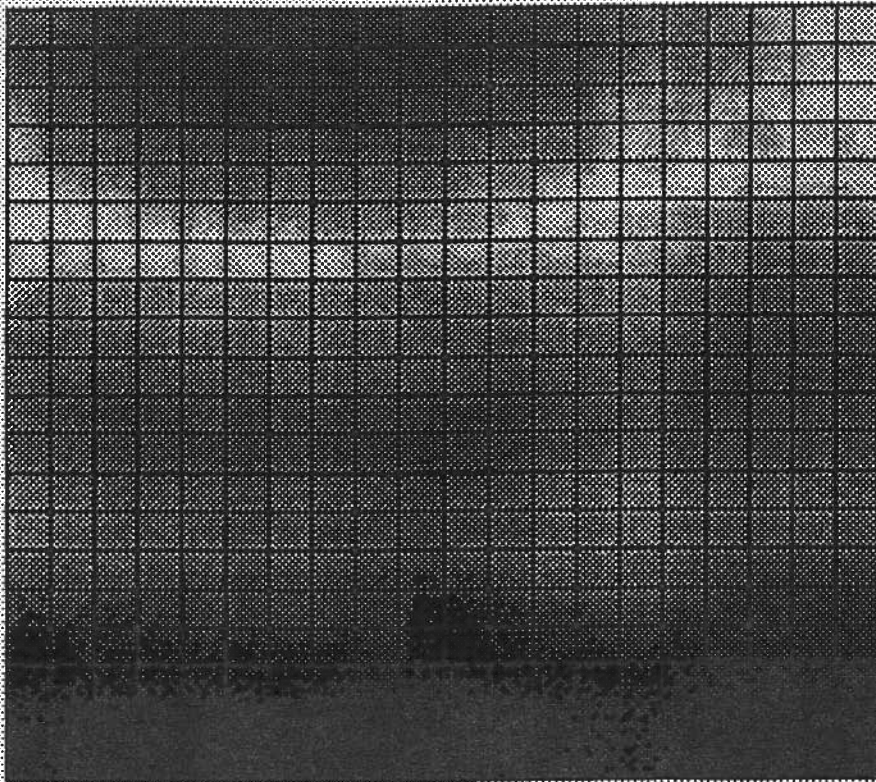


BOUNDARY CONDITIONS:

Input air temp	: 850 K
Input fuel temp	: 850 K
Input flux density oxygen	: 0.55 mol/m ² s
Input flux density hydrogen	: 0.38 mol/m ² s
Stoichiometric ratio	: 2.89
Electrical potential	: 0.76 V/cell
Heat loss	: none

FIGURE 4

SOLID TEMPERATURE - CERAMIC INTERCONNECT



SOLID TEMPERATURE - METALLIC INTERCONNECT

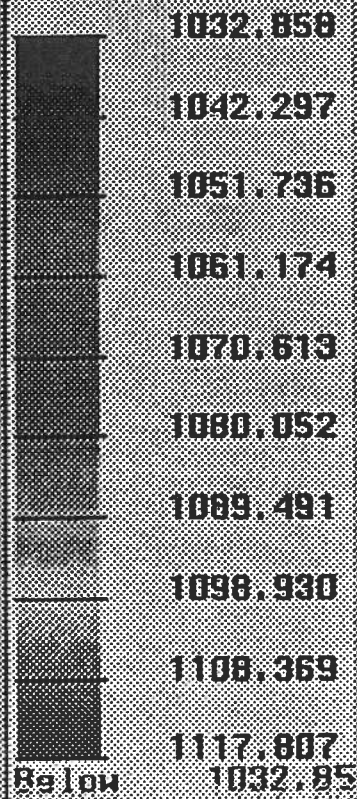
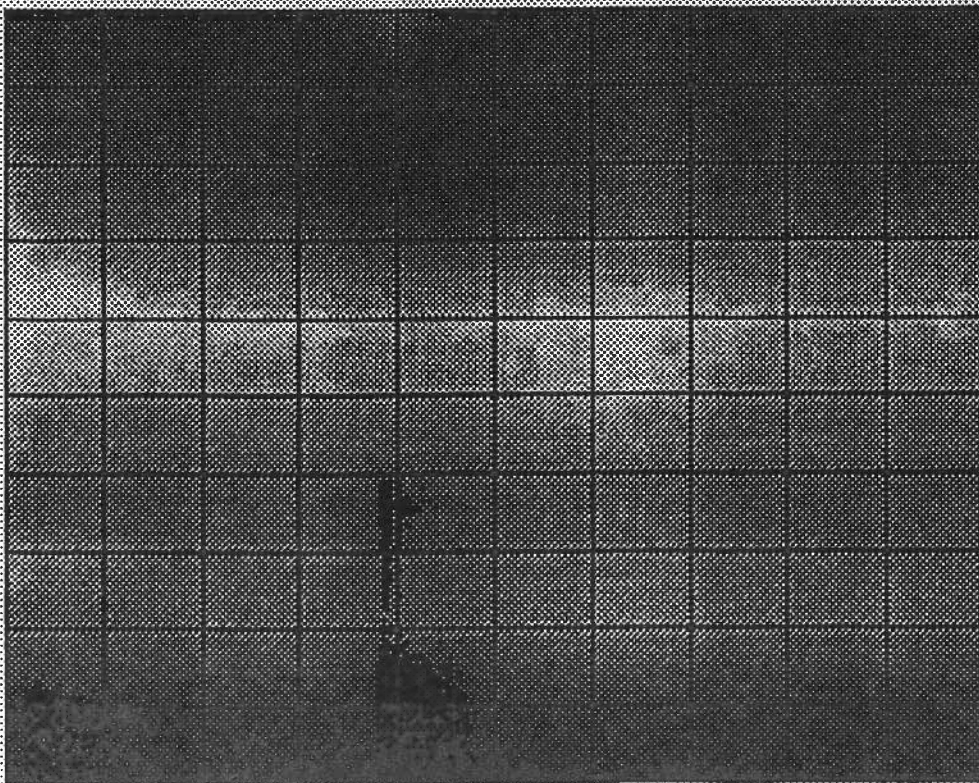
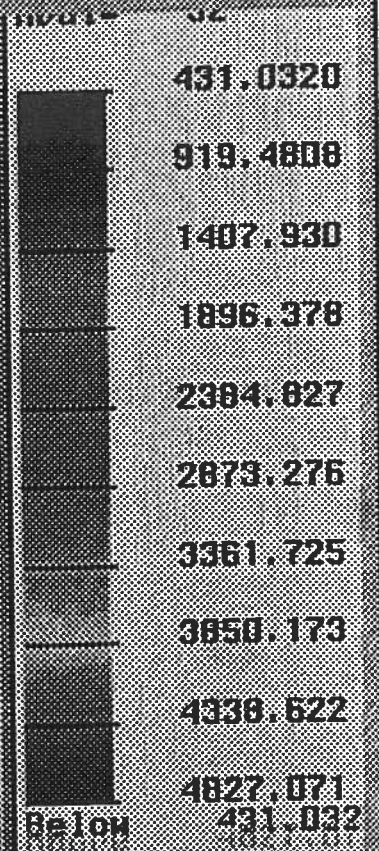
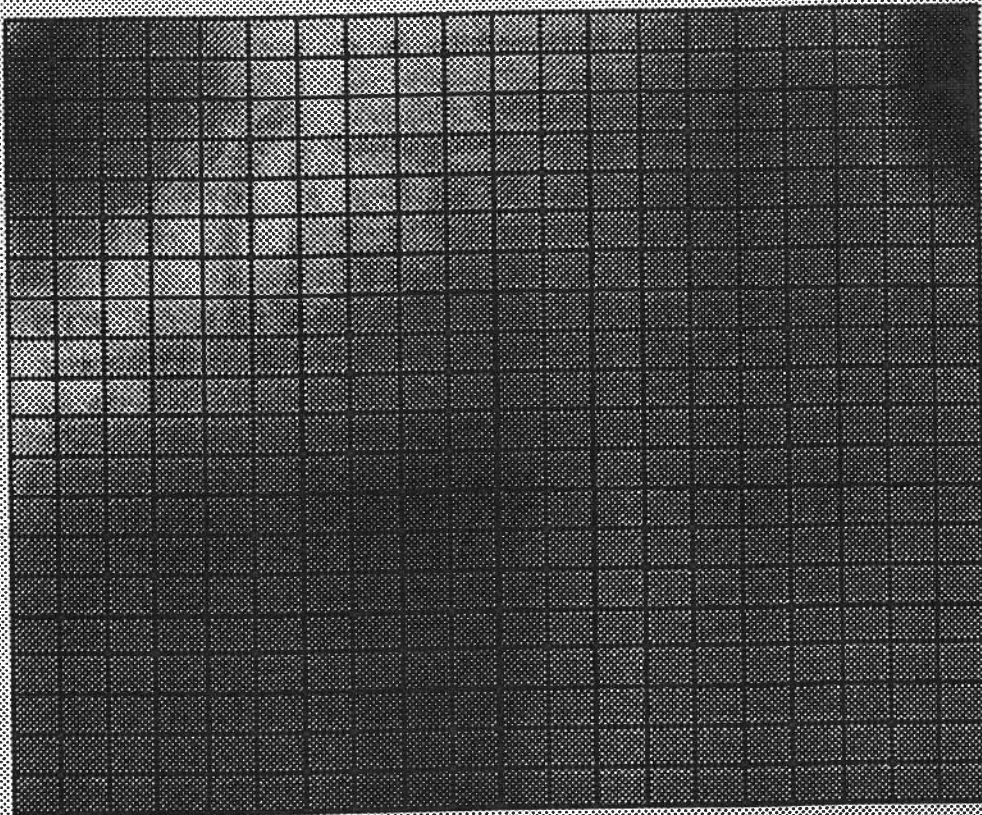
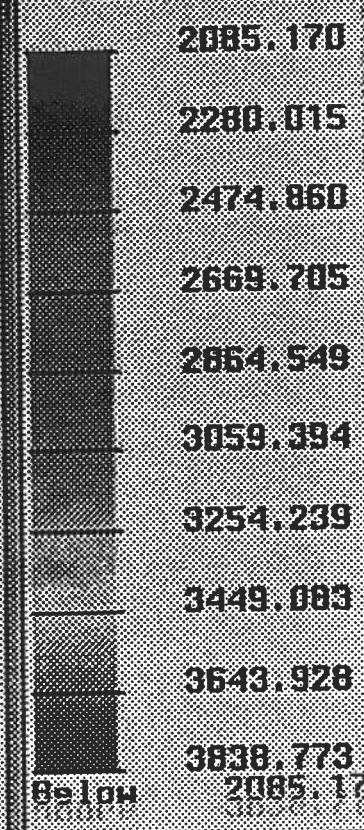
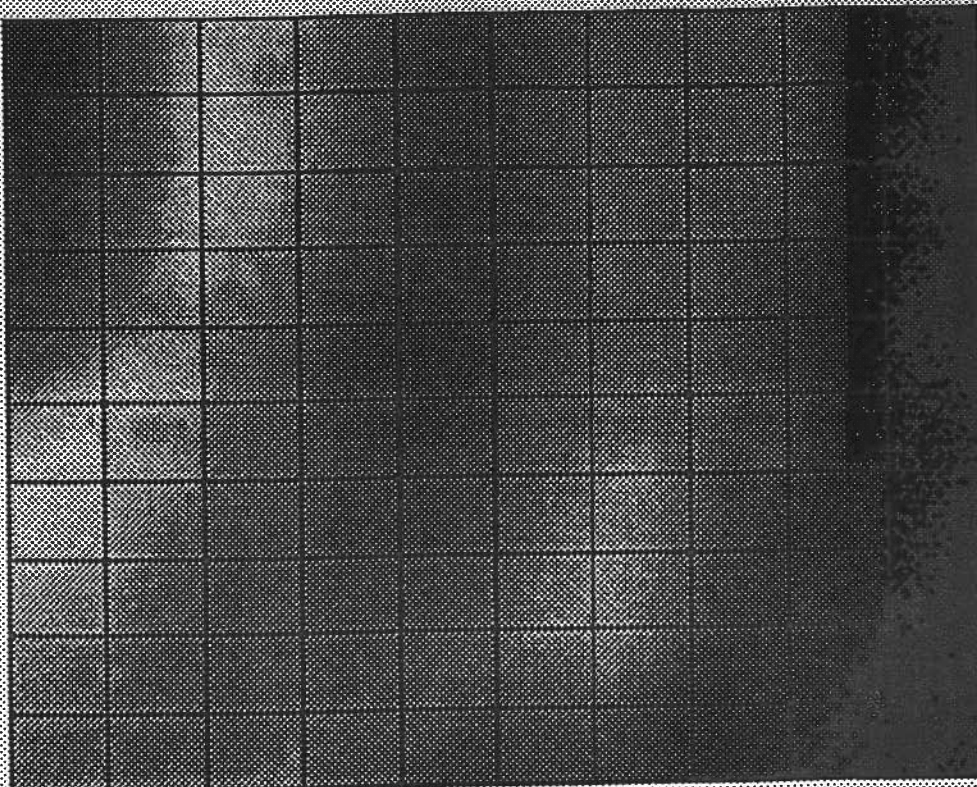


FIGURE 5

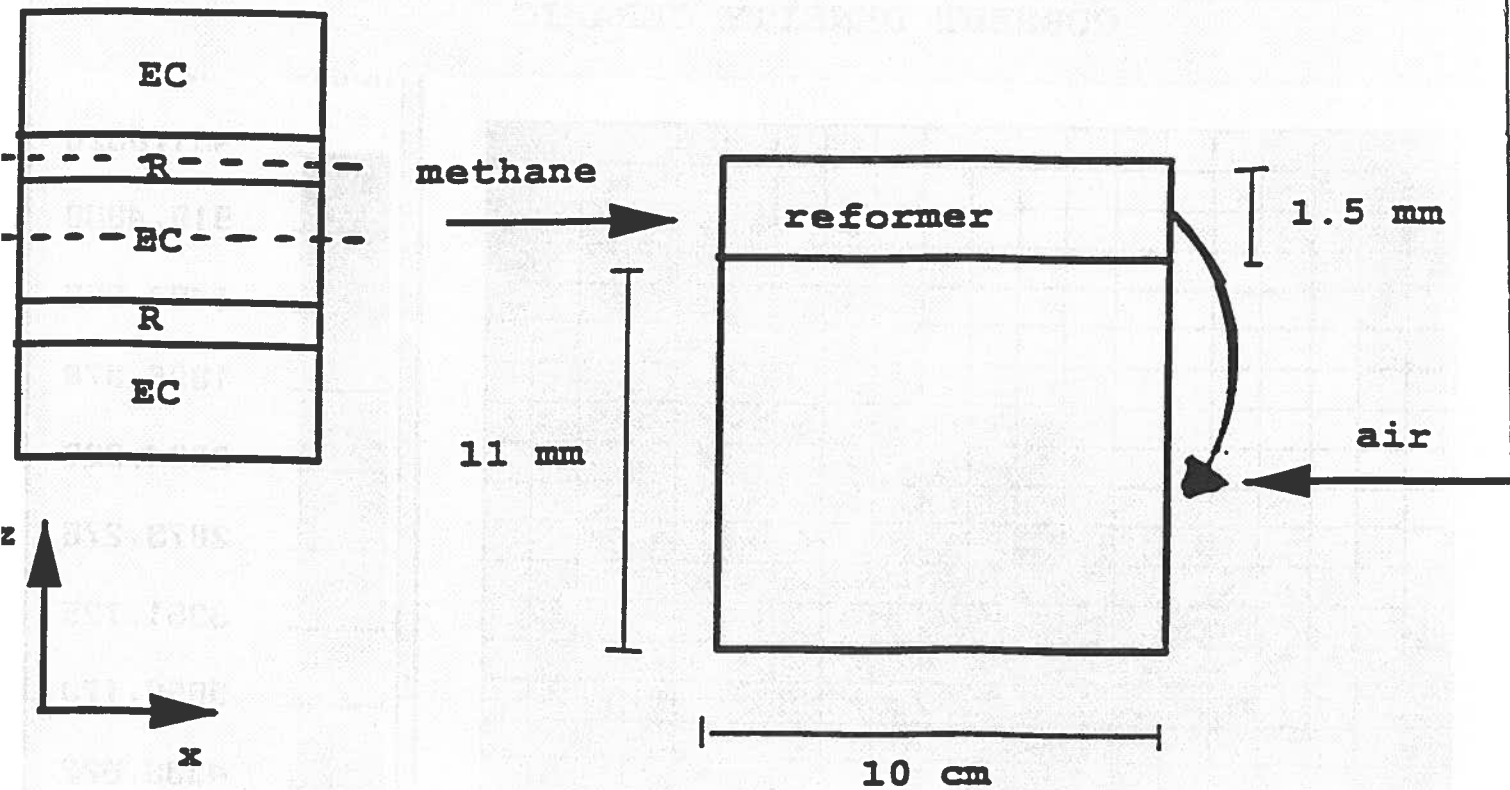
CURRENT DENSITY CERAMIC



CURRENT DENSITY METALLIC



DESCRIPTION OF CASE 3



BOUNDARY CONDITIONS:

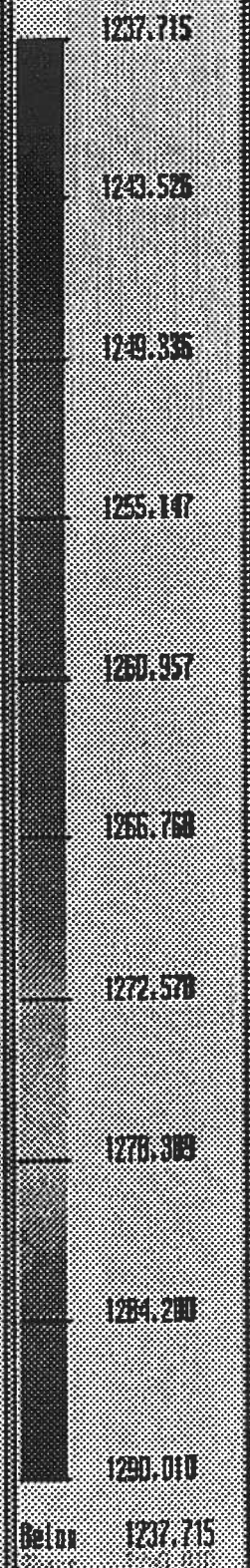
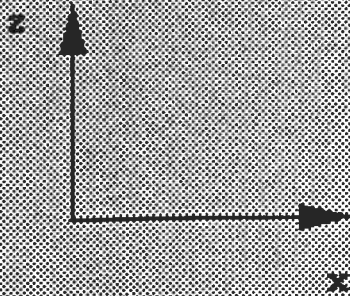
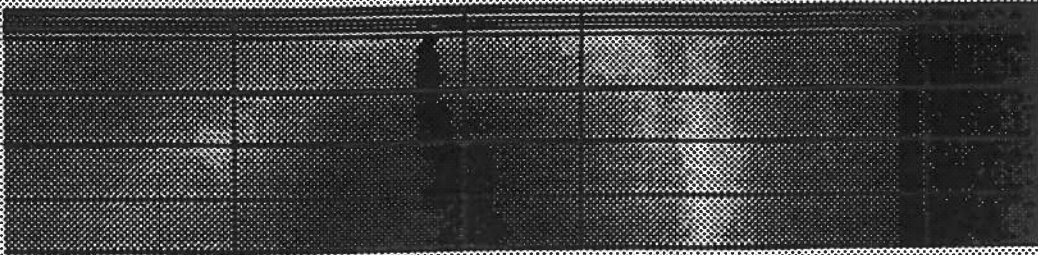
Input air temp (EC zone)	: 1150 K
Input fuel temp (R zone)	: 950 K
Input flux density oxygen	: $0.55 \text{ mol/m}^2\text{s}$
Input flux density methane	: $0.70 \text{ mol/m}^2\text{s}$
Stoichiometric ratio	: 2.85
Electrical potential	: 0.76 V/cell
Heat loss	: none

FIGURE 6

FIGURE 7

SOLID TEMPERATURE PROFILE
Integrated Reforming

field_min 1237.715
field_max 1290.010
sol_min 1237.715
sol_max 1290.010
nnode: 32



	case 1	case 2	case 3
$T_{a,in}$	850 K	775 K	1150 K
$T_{f,in}$	850 K	775 K	950 K
$T_{a,out}$	1188 K	1116 K	1264 K
$T_{f,out}$	1056 K	1084 K	1263 K
$T_{s,min}$	923 K	1033 K	1237 K
$T_{s,max}$	1213 K	1118 K	1290 K
$(\Delta T/\Delta X_i)_{max}$	3676 K/m	1367 K/m	1592 K/m
$U_{f,av}$	0.85	0.88	0.89
$U_{f,min}$	0.68	0.77	0.89
$U_{f,max}$	0.99	0.93	0.89
$\dot{j}_{z,av}$	2751 A/m ²	2838 A/m ²	2928 A/m ²
ΔV	.76 V/cell	.76 V/cell	.76 V/cell

SOFC Two Dimensional "Unit Cell" Modelling

James R. Ferguson*

CH-5401 Baden, Switzerland

Abstract

The governing equations for a two dimensional cross-section of a solid oxide fuel cell (SOFC) are developed describing the distribution of temperature, electrical potential and current flow. The equations giving the distribution of oxygen and hydrogen resulting from diffusion processes in the porous cathode and anode are also developed. The equations are applied to the smallest non-repeating geometrical pattern representing a "unit cell". The electrochemical processes which drive the SOFC appear as boundary conditions to the governing equations since the chemical reactions occur at the electrode-electrolyte interfaces.

The electrochemical boundary conditions cause a jump in the electrical potential across each of the electrode-electrolyte interfaces. This is treated by transforming the problem into a stream function formulation describing the flow of current through the cell. The current is noted to be continuous across the boundaries thus simplifying the problem.

An iterative solution procedure is proposed by which the governing equations can be solved to yield results describing the distribution temperature, current paths, electrical potential, oxygen concentration and hydrogen concentration in each appropriate domain of the cell.

The model developed here can be used to analyze the basic geometry of a solid oxide electrochemical cell upon which a cell stack is based. Losses resulting from diffusion limitations or ohmic resistance can be located and studied providing a means to study the influences of geometry alterations. Furthermore, "equivalent" electrical and thermal conductivities can be deduced from the "unit cell" model upon which stack models can be developed. Due to computational limitations stack models, typically, do not treat the local details which are contained in the "unit cell" model.

* This work sponsored by the Swiss Federal Office of Energy, CH-3003 Bern, Switzerland

1. Introduction

In this report the mathematical equations describing the operation of a solid oxide fuel cell (SOFC) in 2 dimensions are developed. The effort is one part of a coordinated international effort to model SOFC processes to aid the design and manufacture of SOFC components as outlined by the "International Energy Agency Implementing Agreement for a Programme of Research, Development and Demonstration on Advanced Fuel Cells, Annex II Modelling and Evaluation of Advanced Solid Oxide Fuel Cell."

The modelling effort has been divided into two parts: a global model and "unit cell" models. The "unit cell" development models the local details of temperature, electrical potential and current density distributions from which appropriate averages are defined which are in turn used to determine SOFC stack behavior. The global model is being developed to predict temperature, electrical potential and current density distributions of a full SOFC stack. A stack is defined as consisting of multiple electrochemical cells connected in either series or parallel with appropriate fuel and oxidant manifolding. To simplify the computations, the global or "stack" model will be based upon "equivalent" electrical and thermal conductivities for a homogeneous material. Thus the complexities of dealing with the various individual SOFC materials composing an electrochemical cell at the stack level is simplified. The equivalent conductivities are defined as those conductivities which minimize the difference between actual fluxes as determined from a "unit cell" model and the fluxes computed from a model using equivalent conductivities [1].

The objective of the work reported here is to develop the "unit cell" governing equations describing the flux of electrical current and the flux of heat in the parallel flow SOFC bipolar plate geometry. The solution of the equations will yield the local distribution of temperature and electrical potential. The solutions will also provide the necessary data to compute fluxes of current and of heat at "unit cell" boundaries from which "equivalent" thermal and electrical conductivities can be computed. Furthermore, an understanding of the local processes governing the behavior of an SOFC at the cell level will be obtained aiding the design of SOFC components and materials to reduce inefficiencies.

Once several geometrically different "unit cells" have been developed, they may be combined in an appropriate manner to develop SOFC stacks with desired thermal and electrical characteristics. Hence both the "unit cell" and stack models will prove to be useful SOFC design tools.

2. SOFC Unit Cell Geometry

The equations, boundary conditions and solution method developed here will describe the distributions of electrical potential, temperature, current flow and heat flow for the two-dimensional SOFC illustrated in Fig. 1a. The geometry is typical of a bipolar planar SOFC design [2] with an interconnecting plate which electrically connects the cathode of one electrochemical cell with the anode of another electrochemical cell thus providing a series connection. The series connections are necessary to increase the voltage produced by the cell stack.

The geometrical parameters of the two dimensional geometry are defined in Fig. 1b. This is the smallest non-repeating pattern of an SOFC stack. This pattern may be repeated spatially in either the x-, y- or z-directions to build a stack with "unit cells" electrically connected in series or parallel. When the cells are repeated in the channel directions then the unit cells are connected in series with respect to the oxidant and fuel supplies, otherwise the connections are in parallel.

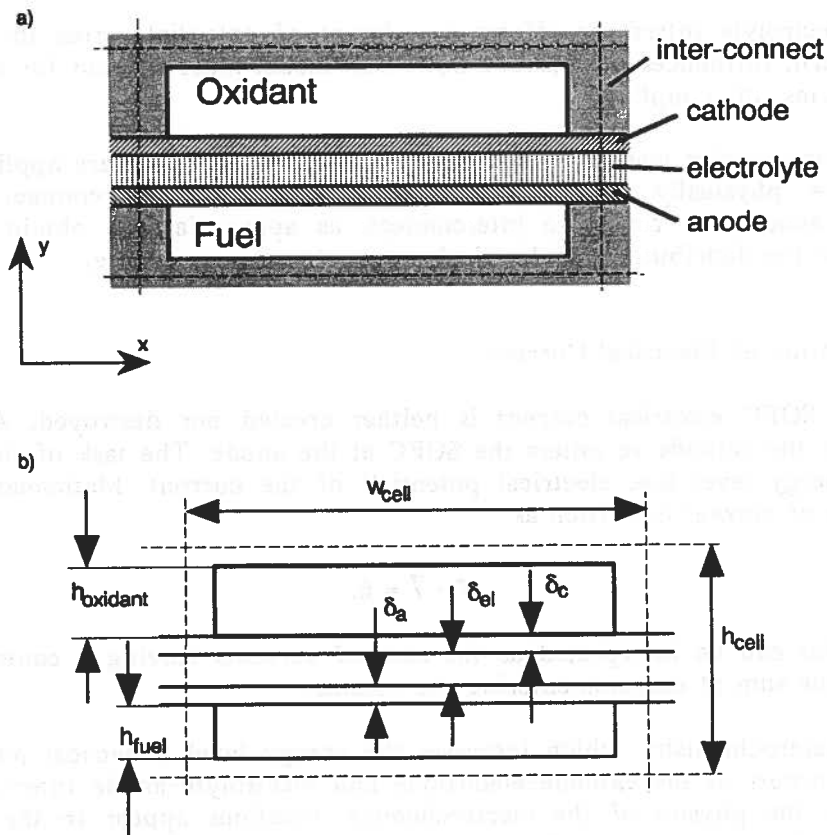


Figure 1. a) SOFC two-dimensional "unit cell" in parallel flow, b) SOFC geometrical parameters.

The two dimensional unit cell geometry offers several significant advantages over a full three dimensional model. The 2-D geometry is computationally less complex, simpler to formulate mathematically and therefore more efficient. The most advantageous point, though, is the ability to mathematically transform the governing equation for electrical potential into an equation describing current flow paths (i.e. a stream function formulation.) The advantage is best observed in the transformed boundary conditions. Many of the unknown constants involved in the potential step at the anode-electrolyte and electrolyte-cathode interfaces disappear thus simplifying the specification of boundary conditions at these interfaces. As a consequence inaccuracies of estimating unknown physical quantities are avoided. This point is explained in more detail in Section 5; Governing Equations and Boundary Conditions.

A further advantage will be realized when a full 3-dimensional model is developed. Unfortunately it is not possible to formulate a stream function for 3-dimensional problems however the solution of the 2-dimensional stream function formulation will indicate certain requirements of the form of the boundary conditions when the problem is formulated in terms of potential for the 3-D case.

3. Conservation Principles

The SOFC problem formulation embodies the conservation of three distinct coupled quantities: electrical current, heat and mass. The flow of current causes the generation of heat through chemical reactions and ohmic resistance heating and the flow of heat causes temperature gradients which spatially alters the electrolytes ionic conductivity thus changing the flow of current. Finally, the diffusion rate of oxygen and fuel through the cathode and anode respectively must balance the flow of current at electrochemical reaction sites. The concentration of oxygen and fuel at the

electrode-electrolyte interfaces affects the change of potential across the interfaces which, in turn, influences the current flow. The model must account for each of the different forms of coupling.

The conservation laws for electrical current, heat and mass are applied to each of the five physically distinct domains: oxidant side interconnect, cathode, electrolyte, anode and fuel side interconnect; as appropriate to obtain governing equations for the distribution of electrical potential and temperature.

3.1 Conservation of Electrical Current

In an SOFC electrical current is neither created nor destroyed. All current which leaves the cathode re-enters the SOFC at the anode. The task of the SOFC is raise the energy level (i.e. electrical potential) of the current. Mathematically, the conservation of current is written as

$$\nabla \cdot \vec{i} = 0. \quad (1)$$

Physically this can be interpreted as the sum of currents leaving a control volume must equal the sum of currents entering the volume.

The electrochemistry which increases the energy level (electrical potential) of the current occurs at the cathode-electrolyte and electrolyte-anode interfaces. As a consequence, the physics of the electrochemical reactions appear in the boundary conditions to the governing equations.

3.2 Conservation of Heat

Due to the flow of electrical current heat is generated on a per unit volume basis due to ohmic resistance in an SOFC. Conservation of thermal energy is written as

$$\nabla \cdot \vec{q} = q''' \quad (2)$$

where \vec{q} is the heat flux vector and q''' is the heat generated per unit volume. This equation can be interpreted physically as the sum of heat leaving a control volume must equal the heat entering the volume plus the heat generated within the volume.

The heat generated by the chemical reactions occurring at the cathode-electrolyte and electrolyte-anode interfaces is surface heat generation and as such does not appear in Eq. 2. Surface heat generation, such as this, appears in the boundary conditions to the governing equations.

3.3 Conservation of Mass

In the porous electrodes of the SOFC chemical species which participate in the electrochemical reactions migrate by molecular diffusion from the channel to the electrode-electrolyte interfaces. Conservation of mass for such movement is written as

$$\nabla \cdot \vec{j}_i = 0 \quad (3)$$

where \vec{j}_i is the molar flux of species i . Physically this equation can be interpreted as the sum of mass leaving a control volume must equal the sum of mass entering the control volume.

4. Physical Laws

The physical laws which relate heat flux, current flux and mass flux to "measurable" quantities are known as Fourier's law of heat conduction, Ohm's law and Fick's law of diffusion. Although there exist molecular interpretations to these laws they are primarily considered to be phenomenological laws based upon vast experimental evidence.

4.1 Ohm's Law

Ohm's law linearly relates the flux of current to the gradient of electric potential, ϕ , and is written as

$$\vec{i} = -\sigma \nabla \phi \quad (4)$$

where σ is the electrical conductivity of the material in the region of interest (note: $\sigma = 1/\rho$, where ρ is the electrical resistivity).

4.2 Fourier's Law of Heat Conduction

Fourier's law of heat conduction linearly relates the heat flux, q , to the gradient of temperature, T , and is written as

$$\vec{q} = -\lambda \nabla T \quad (5)$$

where λ is the thermal conductivity of the material in the region of interest.

4.3 Fick's Law of Diffusion

Fick's Law of diffusion linearly relates the molar flux of a species to the concentration gradient of the species and is written as

$$\vec{J}_i = -c D_{i-j} \nabla x_i + x_i (\vec{J}_i + \vec{J}_j) \quad (6)$$

for a binary mixture where c is the molar concentration of the mixture D is the coefficient of diffusion of species i in j and x_i is the mole fraction of i . The first term on the right hand side of the equation represents the molar flux due to a concentration gradient while the second term represents the flux due to movement of "bulk" fluid.

4.4 Ohmic Heat Generation

The ohmic heat production, q''' , appearing in Eq. 2 can also be derived from Ohm's law. The resistance heating due to electrical current flowing through a material is given by

$$q''' = -\vec{i} \cdot \nabla \phi \quad (7)$$

Substituting Ohm's law for \vec{i} into this equation yields

$$q''' = \sigma \nabla \phi \cdot \nabla \phi \quad (8)$$

for the heat production per unit volume of the material in the region of interest.

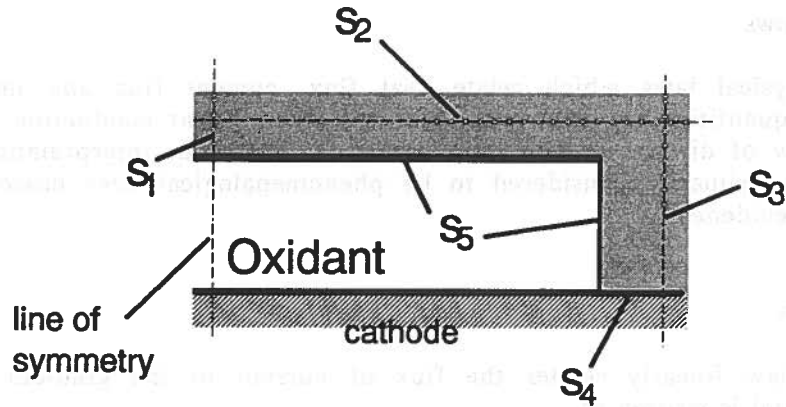


Figure 2. Oxidant side interconnect computational domain.

4.5 Newton's Law of Cooling

Newton's law of cooling is not actually a fundamental phenomenological law but rather a model combining Fourier's law of heat conduction with fluid movement to simplify the description of heat transferred between a body and a fluid. It is an expression often used to describe boundary conditions in heat transfer problems and is written as

$$q = h (T_s - T_f)$$

where q is the heat flux leaving the boundary, h is the heat transfer coefficient, and T_s T_f are the solid boundary and fluid temperatures respectively.

5. Governing Equations and Boundary Conditions

The geometry illustrated in Fig 1. is subdivided into 5 computational domains. Governing equations based upon conservation of electric current and heat which describe the distribution of electric potential and temperature are written for each domain. Conditions are then placed along the boundaries of each domain which are physically realistic to complete the mathematical formulation of the model. The development follows the methods in [3].

In the equations that follow, symmetry has been assumed. The neighboring channels which occur to the left and right of the geometry shown in Fig. 1 are assumed to possess the same fuel and oxidant temperatures and the same fuel and oxidant compositions as the channels in question. The symmetry reduces the size of the computational domain in half simplifying the computations and increasing the accuracy of the results.

5.1 Domain: Oxidant Side Interconnect

The oxidant side interconnect is sketched in Fig. 2 showing the computational domain and boundaries. Due to symmetry, computations need only be made in half of the original domain. Applying the conservation of electrical current and heat principles to this domain and substituting Ohm's and Fourier's laws gives

$$\nabla^2 \phi = 0 \quad (9)$$

$$-\lambda \nabla^2 T = \sigma \nabla \phi \cdot \nabla \phi \quad (10)$$

as governing equations assuming the material properties, σ and λ , are constant.

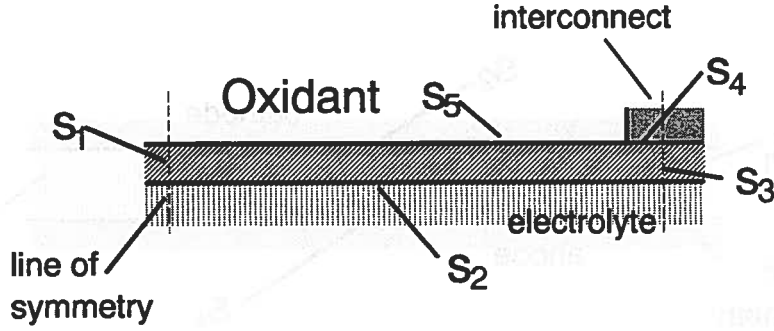


Figure 3. Cathode computational domain.

The boundary conditions for the potential and temperature equations, Eqs. 9 and 10, are relatively straightforward. Along boundaries S_1 and S_3 no current or heat crosses the boundaries due to symmetry considerations ($i_x=0$, $q_x=0$). Along S_2 , a periodic boundary condition is used. The electrical potential and thermal gradients normal to this boundary equal the respective potential and thermal gradients along the companion boundary of the fuel side interconnect ($\nabla\phi=\nabla\phi_{IC_{fuel}}$; $\nabla T=\nabla T_{IC_{fuel}}$). At S_4 , both the electrical potential and temperature must be continuous equalling the potential and temperature in the cathode ($\phi=\phi_c$; $T=T_c$). Along S_5 no current crosses since the oxidant in the channel is a non-conducting medium and the heat transferred to the oxidant channel follows Newton's law of cooling ($\nabla\phi=0$; $\nabla T=h_a(T_{IC}-T_{oxidant})$).

These boundary conditions can be summarized mathematically as follows:

$$\text{Boundary } S_1: \quad \nabla\phi \cdot n = 0 \quad \nabla T \cdot n = 0 \quad (11)$$

$$\text{Boundary } S_2: \quad \nabla\phi \cdot n = \nabla\phi_{IC_{fuel}} \cdot n \quad \nabla T \cdot n = \nabla T_{IC_{fuel}} \cdot n \quad (12)$$

$$\text{Boundary } S_3: \quad \nabla\phi \cdot n = 0 \quad \nabla T \cdot n = 0 \quad (13)$$

$$\text{Boundary } S_4: \quad \phi = \phi_{cathode} \quad T = T_{cathode} \quad (14)$$

$$\text{Boundary } S_5: \quad \nabla\phi \cdot n = 0 \quad \nabla T \cdot n = h_a(T - T_{oxidant}) \quad (15)$$

where n is the outward pointing unit vector normal to the surface. Unless otherwise subscripted the dependent variables are to be taken within the oxidant side interconnect domain.

5.2 Domain: Cathode

The computational domain for the cathode is illustrated in Fig. 3 reflecting the symmetry assumption. In this domain the three conservation principles are applied. Substituting Ohm's, Fourier's and Fick's laws into the current, heat and mass conservation equations gives

$$\nabla^2\phi = 0 \quad (16)$$

$$-\lambda\nabla^2 T = \sigma \nabla\phi \cdot \nabla\phi \quad (17)$$

$$\nabla \cdot \left[\frac{1}{1-x_{O_2}} \nabla x_{O_2} \right] = 0 \quad (18)$$

for constant material properties, σ and λ . In writing Eq. 18, use has been made of $j_{N_2}=0$. In the cathode, there is no net flow of nitrogen and oxygen is observed to be diffusing through a "stagnant" gas film.

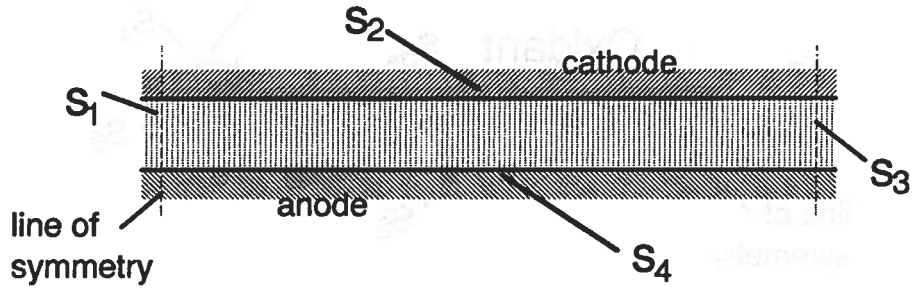


Figure 4. Electrolyte computational domain.

The boundary conditions for Eqs. 16, 17 and 18 are written without difficulty. Due to symmetry, the conserved fluxes, electrical current, mass flux and heat do not cross boundaries S_1 and S_3 . Along S_2 , the potential differs from the potential in the electrolyte by ϕ_{Nc} (see Eq. 34 and the discussion of the potential jumps), the flux of oxygen crossing the boundary equals one half of the ionic current in the electrolyte normal to the boundary ($j_{yO_2} = 4Fi_{yel}$; see electrochemical reactions in Section 5.3) and the temperature is continuous ($T = T_{el}$). At S_4 , the electrical potential is continuous ($\phi = \phi_{IC}$), no mass crosses the boundary and the temperature is continuous ($T = T_{IC}$). Along S_5 , no current crosses the boundary, the mole fraction of oxygen is specified and the heat transferred to the oxidant channel is described by Newton's law of cooling. Mathematically, these conditions can be summarized as:

$$\text{Boundary } S_1: \quad \nabla\phi \cdot \mathbf{n} = 0 \quad \nabla T \cdot \mathbf{n} = 0 \quad \nabla x_{O_2} \cdot \mathbf{n} = 0 \quad (19)$$

$$\text{Boundary } S_2: \quad \phi = \phi_{el} - \phi_{Nc} \quad T = T_{el} \quad \frac{c D_{O_2-N_2}}{1-x_{O_2}} \nabla x_{O_2} = 4F(\sigma \nabla \phi)_{el} \quad (20)$$

$$\text{Boundary } S_3: \quad \nabla\phi \cdot \mathbf{n} = 0 \quad \nabla T \cdot \mathbf{n} = 0 \quad \nabla x_{O_2} \cdot \mathbf{n} = 0 \quad (21)$$

$$\text{Boundary } S_4: \quad \phi = \phi_{IC} \quad T = T_{IC} \quad \nabla x_{O_2} \cdot \mathbf{n} = 0 \quad (22)$$

$$\text{Boundary } S_5: \quad \nabla\phi \cdot \mathbf{n} = 0 \quad \nabla T \cdot \mathbf{n} = h_a(T - T_{oxidant}) \quad x_{O_2} = x_{O_2oxidant} \quad (23)$$

where \mathbf{n} is the outward pointing unit vector normal to the surface. Unless otherwise subscripted, the dependent variables are taken to be as part of the cathode computational domain.

The constant $D_{O_2-N_2}$ found in Eq. 20 is the effective diffusion coefficient for oxygen diffusing through the cathode. In general it is a function of ϵ , the cathode porosity, d , pore diameter, τ , pore tortuosity, and $D'_{O_2-N_2}$ the diffusion coefficient in the pure gaseous state. In the absence of experimentally determined values, the effective diffusion coefficient may be approximated by

$$D_{O_2-N_2} = D'_{O_2-N_2} \epsilon^n / \tau \quad (24)$$

where $1.0 \leq n \leq 1.5$.

5.3 Domain: Electrolyte

The electrolyte and its computational domain with boundaries are shown in Fig. 4. In this domain all electrochemical reactions are assumed to occur at boundaries S_2 and S_4 . The reduction of oxygen occurs at S_2 to create O^- ions while

the oxidation of hydrogen occurs at S_4 to generate water vapor, electrons and heat. Within the domain the conservation of current and heat principles apply. Substituting Ohm's and Fourier's laws into the conservation equations, Eqs. 1 and 2, yields

$$\nabla \cdot (\sigma \nabla \phi) = 0 \quad (25)$$

$$-\lambda \nabla^2 T = \sigma \nabla \phi \cdot \nabla \phi \quad (26)$$

where the electrolyte's conductivity, σ , is a function of position due to its temperature sensitivity but λ , the thermal conductivity, is assumed to be constant.

The choice of boundary conditions is problematic for the description of electric potential, Eq. 25, but rather straightforward for the temperature field modelled by Eq. 26. The temperature field boundary conditions are treated first.

Due to symmetry, there is no flux of heat crossing boundaries S_1 or S_3 ($\nabla T = 0$). Along boundary S_2 the temperature must be continuous ($T = T_c$) and along boundary S_4 the sum of heat fluxes in the electrolyte and anode at the interface must equal the chemical heat generation at the interface ($q_{el} + q_a = q''$). The heat generated at the interface is given by

$$q'' = -i_y T \Delta S_{H_2O} / 2F = (\sigma \nabla \phi \cdot n)_a T \Delta S_{H_2O} / 2F \quad (27)$$

The thermal boundary conditions for the electrolyte can be summarized mathematically as

$$\text{Boundary } S_1: \quad \nabla T \cdot n = 0 \quad (28)$$

$$\text{Boundary } S_2: \quad T = T_c \quad (29)$$

$$\text{Boundary } S_3: \quad \nabla T \cdot n = 0 \quad (30)$$

$$\text{Boundary } S_4: \quad -\lambda \nabla T \cdot n = (\lambda T \cdot n)_a + (\sigma \nabla \phi \cdot n)_a T \Delta S_{H_2O} / 2F \quad (31)$$

The boundary conditions for the electric potential along boundaries S_1 and S_3 result from symmetry, namely that no current crosses the boundaries ($\nabla \phi = 0$). The boundary conditions along the remaining boundaries, S_2 and S_4 , are complicated by the electrochemistry occurring at the electrode-electrolyte interfaces. Along S_2 the chemical reaction



occurs causing a discontinuous potential jump across the cathode-electrolyte interface. Similarly, along S_4 the chemical reaction



occurs causing a potential jump at the electrolyte-anode interface. The potential jump at each of the interfaces is given by the respective Nernst potentials for the chemical reactions in Eqs. 32 and 33. Namely,

$$\text{cathode: } \phi_e = \phi_c + \phi_{Nc}, \quad \phi_{Nc} = [-\Delta G_{f32} - \{\mu_{O^-} - (\frac{1}{2}\mu_{O_2} + 2\mu_{e^-})\}] / 2F \quad (34)$$

$$\text{anode: } \phi_e = \phi_a - \phi_{Na}, \quad \phi_{Na} = [-\Delta G_{f33} - \{(\mu_{H_2O} + 2\mu_{e^-}) - (\mu_{H_2} + \mu_{O^-})\}] / 2F \quad (35)$$

where ΔG_f is the Gibbs free energy of formation for the respective reactions. The sum of the two Nernst potentials gives

$$\phi_N = [-\Delta G_f - RT \ln(p_{H_2O}/(p_{H_2} + p_{O_2}^{1/2}))]/2F \quad (36)$$

the Nernst potential for the electrochemical oxidation of hydrogen. In writing Eq. 36 the ideal gas expressions for the chemical potential of hydrogen and oxygen have been used ($\mu_i = RT \ln(p_i)$, where p is the partial pressure of component i).

The difficulty with the boundary condition specification is reflected in Eqs. 34 and 35. The chemical potentials of O^* in the electrolyte and e^- in the cathode and anode are not known although the Nernst potential is known for the net reaction ($H_2 + \frac{1}{2}O_2 \rightarrow H_2O$). Furthermore, the measurement of these quantities is not a trivial matter. It is important to estimate the potential jump accurately since this will affect the current flow paths and the ohmic losses occurring along the paths.

In this two dimensional formulation a solution to this problem is obtained by transforming the potential equation, Eq. 25, into a stream function formulation using the transformations,

$$\frac{\partial \phi}{\partial x} = \frac{\partial \varphi}{\partial y} \quad \frac{\partial \phi}{\partial y} = -\frac{\partial \varphi}{\partial x} \quad (37)$$

The current flux is related to the stream function by

$$i_x = -\sigma \frac{\partial \phi}{\partial x} = -\sigma \frac{\partial \varphi}{\partial y} \quad i_y = -\sigma \frac{\partial \phi}{\partial y} = \sigma \frac{\partial \varphi}{\partial x} \quad (38)$$

The governing equation becomes,

$$\frac{\partial}{\partial x} \left[\sigma \frac{\partial \varphi}{\partial x} \right] + \frac{\partial}{\partial y} \left[\sigma \frac{\partial \varphi}{\partial y} \right] = 0 \quad (39)$$

which is equivalent to saying the current flow is irrotational. The stream function is best interpreted as the function which describes current paths. Lines of $\varphi = \text{constant}$ represent current paths through the domain. The difference between two φ values represents the total current flowing parallel and between the two φ paths. Once the stream function formulation has been solved, the potential distribution can be computed with the use of Eqs. 37.

The boundary conditions are now simpler to formulate. Along boundary S_1 , φ is arbitrarily given a value of 0 and along S_3 , φ is set equal to the total current flowing through the unit cell, i_{total} . Along boundaries S_2 and S_4 , the derivative normal to the boundary is specified using Eq. 37. The boundary conditions become

$$S_2, \text{ cathode:} \quad \frac{\partial \varphi}{\partial y} = \frac{\partial \phi_{el}}{\partial x} = \frac{\partial \phi_c}{\partial x} + \frac{1}{2F} \left[-\frac{\partial \mu_{O^*}}{\partial x} + \frac{1}{2} \frac{\partial \mu_{O_2}}{\partial x} + 2 \frac{\partial \mu_{e^-}}{\partial x} \right] \quad (40)$$

$$S_4, \text{ anode:} \quad \frac{\partial \varphi}{\partial y} = \frac{\partial \phi_{el}}{\partial x} = \frac{\partial \phi_a}{\partial x} + \frac{1}{2F} \left[\frac{\partial \mu_{H_2O}}{\partial x} + 2 \frac{\partial \mu_{e^-}}{\partial x} - \frac{\partial \mu_{H_2}}{\partial x} - \frac{\partial \mu_{O^*}}{\partial x} \right] \quad (41)$$

The gradients of the chemical potentials are related to currents through the relations

$$\frac{1}{2F} \frac{\partial \mu_{O^*}}{\partial x} = \left[-\frac{1}{\sigma} i_x \right]_{el} = \frac{\partial \varphi}{\partial y} \quad (42)$$

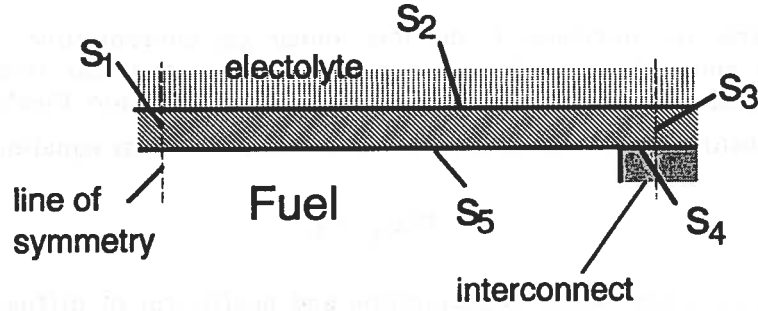


Figure 5. Anode computational domain.

$$\frac{1}{F} \frac{\partial \mu_{e^-}}{\partial x} = \left[-\frac{1}{\sigma} i_x \right]_{c;a} = \frac{\partial \phi_{c;a}}{\partial x} \quad (43)$$

The boundary conditions for the stream function formulation can now be mathematically summarized as (after some algebraic manipulation)

$$\text{Boundary } S_1: \quad \phi = 0 \quad (44)$$

$$\text{Boundary } S_2: \quad \frac{\partial \phi}{\partial y} = \frac{\partial \phi_c}{\partial x} + \frac{RT}{8F} \frac{1}{p_{O_2}} \frac{\partial p_{O_2}}{\partial x} \quad (45)$$

$$\text{Boundary } S_3: \quad \phi = i_{\text{total}} \quad (46)$$

$$\text{Boundary } S_4: \quad \frac{\partial \phi}{\partial y} = \frac{\partial \phi_a}{\partial x} + \frac{RT}{4F} \left[\frac{1}{p_{H_2O}} \frac{\partial p_{H_2O}}{\partial x} - \frac{1}{p_{H_2}} \frac{\partial p_{H_2}}{\partial x} \right] \quad (47)$$

The stream function formulation conveniently avoids the specific specification of the potential jump at the electrode-electrolyte interfaces. In essence, this occurs since the current across the interface must be continuous and, in general, more is known about the flow of current through the "unit cell" than the distribution of electrical potential. For consistency the electrical potential formulation in the other 4 computational domains should also be transformed into a stream function formulation. Making the boundary conditions correspond between domains is then simpler. This is a straight forward mathematical exercise. The results are presented in the Appendix.

5.4 Domain: Anode

The sketch defining the computational domain for the anode is given in Fig. 5. The governing equations describing the variation of electrical potential and temperature in this domain are the same as the equations developed for the cathode except for material constants. The equations are

$$\nabla^2 \phi = 0 \quad (48)$$

$$-\lambda \nabla^2 T = \sigma \nabla \phi \cdot \nabla \phi \quad (49)$$

assuming constant material properties.

Applying Fick's law of diffusion and the conservation of mass principle to the anode to describe the variation of hydrogen mole fraction produces a different result compared to the cathode mass conservation description. Unlike the cathode, the anode hydrogen does not diffuse through a stagnant second component. Due to the electrochemical oxidation of hydrogen at the anode-electrolyte interface, water vapor is diffusing from the interface towards the fuel channel against the diffusion of

hydrogen towards the interface. If the total molar gas concentration, c , is constant throughout the anode then the flux of water vapor is equal to the flux of hydrogen but in the opposite direction ($\dot{j}_{\text{H}_2\text{O}} = -\dot{j}_{\text{H}_2}$). Introducing this into Fick's law, solving for \dot{j}_{H_2} and substituting the result into the conservation of mass equation yields

$$\nabla^2 x_{\text{H}_2} = 0 \quad (50)$$

assuming a constant total molar concentration and coefficient of diffusion. The mole fraction of water vapor is then found quite easily knowing $x_{\text{H}_2} + x_{\text{H}_2\text{O}} = 1$.

The boundary conditions for Eqs. 48,49 and 50 are similar to those given for the cathode. Due to symmetry, electrical current, mass flux and heat do not cross boundaries S_1 and S_3 . Along S_2 , the potential differs from the potential in the electrolyte by ϕ_{Na} , (see Eq. 35), the flux of hydrogen crossing the boundary equals the ionic current in the electrolyte normal to the boundary ($\dot{j}_{\text{yH}_2} = 2Fi_{\text{yel}}$; see electrochemical reactions in Section 5.3) and the heat flux must equal the heat flux from the electrolyte plus the heat generated by the chemical reactions at the anode-electrolyte interface ($q = q_{\text{el}} + i_{\text{y}} T \Delta S / 2F$). At S_4 , the electrical potential is continuous ($\phi_a = \phi_{\text{IC}}$), no mass crosses the boundary ($\dot{j}_{\text{yH}_2} = 0$) and the temperature is continuous ($T = T_{\text{IC}}$). Along S_5 , no current crosses the boundary, the mole fraction of hydrogen is specified and the heat transferred to the fuel channel is described by Newton's law of cooling. Mathematically, these conditions can be summarized as:

$$\text{Boundary } S_1: \quad \nabla \phi \cdot \mathbf{n} = 0 \quad \nabla T \cdot \mathbf{n} = 0 \quad \nabla x_{\text{H}_2} \cdot \mathbf{n} = 0 \quad (51)$$

$$\text{Boundary } S_2: \quad \phi = \phi_{\text{el}} + \phi_{\text{Na}} \quad \sigma \nabla T \cdot \mathbf{n} = (\sigma \nabla T \cdot \mathbf{n})_{\text{el}} + \frac{c D_{\text{H}_2-\text{H}_2\text{O}}}{1-x_{\text{H}_2}} \nabla x_{\text{H}_2} = (-\sigma \nabla \phi \cdot \mathbf{n}) T \Delta S_{\text{H}_2\text{O}} / 2F \quad 2F(\sigma \nabla \phi)_{\text{el}} \quad (52)$$

$$\text{Boundary } S_3: \quad \nabla \phi \cdot \mathbf{n} = 0 \quad \nabla T \cdot \mathbf{n} = 0 \quad \nabla x_{\text{H}_2} \cdot \mathbf{n} = 0 \quad (53)$$

$$\text{Boundary } S_4: \quad \phi = \phi_{\text{IC}} \quad T = T_{\text{IC}} \quad \nabla x_{\text{H}_2} \cdot \mathbf{n} = 0 \quad (54)$$

$$\text{Boundary } S_5: \quad \nabla \phi \cdot \mathbf{n} = 0 \quad \nabla T \cdot \mathbf{n} = h_f (T - T_{\text{fuel}}) \quad x_{\text{H}_2} = x_{\text{H}_2\text{fuel}} \quad (55)$$

where \mathbf{n} is the outward pointing unit vector normal to the surface. Unless otherwise subscripted, the dependent variables are taken to be as part of the anode computational domain.

As with the cathode, the effective diffusion coefficient, $D_{\text{H}_2-\text{H}_2\text{O}}$, is in general a function of the anode porosity, ε , pore diameter, d , and tortuosity, τ . If experimentally measured values are lacking, $D_{\text{H}_2-\text{H}_2\text{O}}$ may, as in the cathode estimation of the effective diffusion coefficient, be estimated from

$$D_{\text{H}_2-\text{H}_2\text{O}} = D'_{\text{H}_2-\text{H}_2\text{O}} \varepsilon^n / \tau \quad (56)$$

where $D'_{\text{H}_2-\text{H}_2\text{O}}$ is the diffusion coefficient in the gaseous state and n is an empirically determined constant.

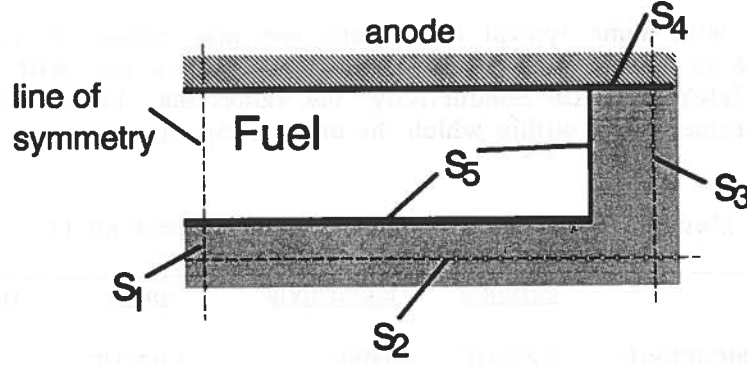


Figure 6. Fuel side interconnect computational domain.

5.5 Domain: Fuel Side Interconnect

The computational domain and boundaries of the fuel side interconnect are shown in Fig. 6. The governing equations in this domain describing the distribution of electrical potential and temperature are the same as in the oxidant side interconnect domain. The governing equations are

$$\nabla^2 \phi = 0 \quad (57)$$

$$-\lambda \nabla^2 T = \sigma \nabla \phi \cdot \nabla \phi \quad (58)$$

assuming constant material properties.

The boundary conditions for Eqs. 57 and 58 are similar to the boundary conditions given for the oxidant side interconnect, Eqs. 11 to 15. No heat crosses the boundaries at S_1 and S_3 due to symmetry ($i_x=0, q_x=0$). A periodic boundary condition on potential and temperature is specified along S_2 to match the boundary condition used for the oxidant side interconnect ($\nabla \phi = \nabla \phi_{IC_{Oxidant}}, \nabla T = \nabla T_{IC_{Oxidant}}$). Along S_4 both the temperature and electric potential must be continuous ($\phi = \phi_a, T = T_a$). At S_5 , no current crosses the boundary and the heat transferred to the fuel channel is given by Newton's law of cooling ($\nabla \phi = 0; \nabla T = h_f(T - T_{oxidant})$).

These boundary conditions can be summarized mathematically as follows:

$$\text{Boundary } S_1: \quad \nabla \phi \cdot \mathbf{n} = 0 \quad \nabla T \cdot \mathbf{n} = 0 \quad (59)$$

$$\text{Boundary } S_2: \quad \nabla \phi = \nabla \phi_{IC_{Oxidant}} \quad \nabla T = \nabla T_{IC_{Oxidant}} \quad (60)$$

$$\text{Boundary } S_3: \quad \nabla \phi \cdot \mathbf{n} = 0 \quad \nabla T \cdot \mathbf{n} = 0 \quad (61)$$

$$\text{Boundary } S_4: \quad \phi = \phi_{anode} \quad T = T_{anode} \quad (62)$$

$$\text{Boundary } S_5: \quad \nabla \phi \cdot \mathbf{n} = 0 \quad \nabla T \cdot \mathbf{n} = h_f(T - T_{fuel}) \quad (63)$$

where \mathbf{n} is the outward pointing unit vector normal to the surface. Unless otherwise subscripted the dependent variables are to be taken within the fuel side interconnect domain.

6. Material Properties and Constants

The solution of the above equations is dependent upon knowing material properties for the various domains and thermodynamic constants. These values can be found throughout the literature. Typical values have been collected and presented in

Table 1 along with some typical dimensions one may expect of the "unit cell". Generally speaking the values are functions of temperature but, with the exception for the electrolyte's electrical conductivity, the values may be considered constant over the temperature range within which the unit cell operates.

Table 1. SOFC Material Properties and Thermodynamic Constants [3]

	<u>cathode</u>	<u>electrolyte</u>	<u>anode</u>	<u>interconnect</u>
electrical conductivity ($\sigma = \Omega^{-1}m^{-1}$)	1.27×10^4	$33400 \times e^{-10300/T}$	3.03×10^4	3.07×10^3
thermal conductivity ($\lambda = W/m-K$)	3.5	2.0	3.0	3.5
thickness ($\delta = \mu$)	50-150	50-300	25-100	200-2000
porosity (ϵ)	0.3-0.5		0.3-0.5	
tortuosity (τ)	~1.5		~1.5	
diffusion coefficient ($D' = cm^2/s$)	$D'_{O_2-N_2} \sim 2.5$		$D'_{H_2-H_2O} \sim 14.5$	
channel width = 0.5-10 mm total cell height = 1.5-5 mm	Universal Gas Constant, $R = 8.314 J/mol-K$ Faraday Constant, $F = 9.648 \times 10^4 C/mol$			

7. Proposed Solution Procedure

The equations developed in the preceding sections describing the variation of temperature, oxygen and hydrogen mole fractions, electric potential and current flow paths need to be solved in an iterative manner due to the non-linearity and coupling of the equations in the 5 domains. A solution procedure is proposed in Fig. 7. This solution procedure is similar in concept to a procedure used successfully to compute temperature and current density distributions in a planar cross-flow SOFC configuration [4]

The scheme separates the solution procedure into two parts. The first half of the scheme solves the electrical problem for given temperature distribution in each domain. In the first iteration the temperature is assumed to be constant throughout each domain. Once the electrical problem has converged, the solution would be considered the constant temperature "solution."

The scheme would then proceed to the second half solving the thermal problem. The thermal problem is solved by computing the temperature distribution in each successive domain beginning with the electrolyte. In these computations the heat source terms appearing in the equations, which are proportional to the square of the current, are considered constant (i.e. the current distribution is not altered although the electrolyte's electric conductivity is temperature sensitive.)

Once the thermal solution has converged, convergence of the entire scheme is checked. If convergence has not been achieved, the procedure is repeated by returning to the solution of the electrical problem followed by the thermal problem. If the solution procedure begins to show signs of instability, stability may be achieved by introducing a relaxation factor. The relaxation factor limits the change

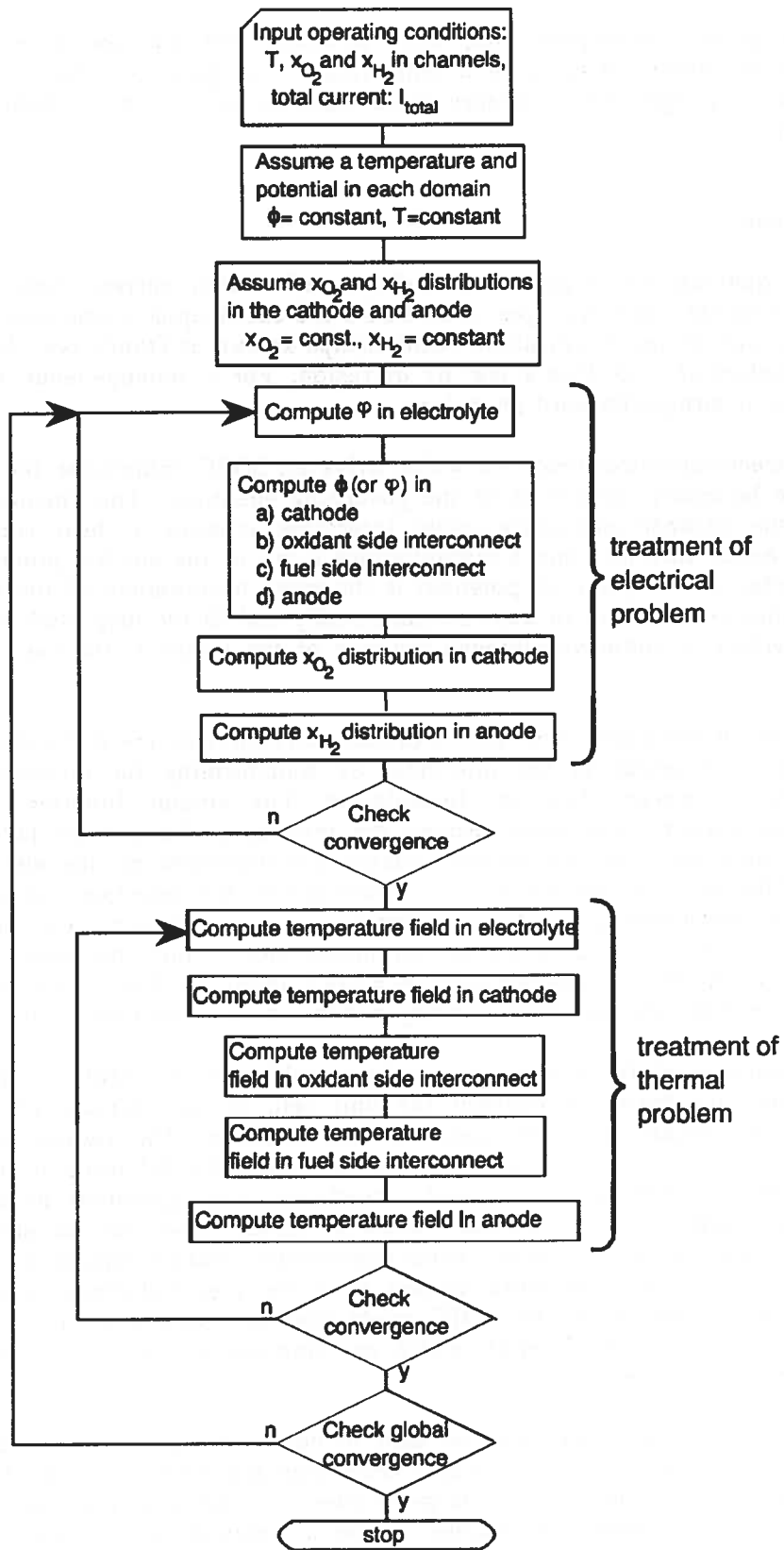


Figure 7. Flow chart of proposed solution procedure.

the solutions can have from their previous values. The relaxation procedure is a standard numerical technique to make non-convergent solution procedures convergent.

Once global convergence has been achieved, the solution gives the spatial distribution of electric potential and temperature throughout the "unit cell" and the distribution of oxygen and hydrogen mole fractions within the cathode and anode respectively.

8. Conclusions

The equations which govern the behavior of electric current, flow of heat and diffusion of oxygen and hydrogen in an SOFC are based upon conservation principles with application of the constitutive relationships known as Ohm's law, Fourier's law of heat conduction and Fick's law of diffusion. For a homogeneous medium the development is straightforward procedure.

The electrochemical reactions which drive an SOFC complicate the analysis by altering the boundary conditions of the governing equations. The chemical reactions occur at the cathode-electrolyte-anode interfaces creating a heat source at the electrolyte-anode interface and a discontinuous jump of the electric potential at each of the interfaces. The jump of potential is the more troublesome of the two since i) discontinuities are difficult to treat mathematically and ii) the magnitude of the jump at each interface is unknown although the sum of the jumps at the two interfaces is known.

The two-dimensional "unit cell" treatment circumvents the difficulties involved with jumps of potential at the interfaces by transforming the electrical potential problem into a stream function formulation. The stream function formulation describes the current flow paths. Across the interfaces, the current paths must be continuous since electrons are neither created nor destroyed by the electrochemical reactions. This fact, the continuity of current across the interfaces, is exploited to transform the mathematically difficult jump of potential boundary conditions and the associated unknown chemical potential parameters into a more manageable condition on the flow of current. In essence more is known about the flow of current than the distribution of electrical potential allowing a more accurate solution of the problem.

The solution of the governing equations yields the temperature, current path, and potential distribution throughout the unit cell. In the cathode and anode the distribution of oxygen and hydrogen are also obtained. The results will indicate where losses are occurring. If cell operation is limited by diffusion of the reactive species to the cathode-electrolyte-anode interfaces, large gradients of oxygen and hydrogen will appear in the solution. Likewise, ohmic losses can be identified and quantified. Locations where current paths concentrate indicate regions of high ohmic loss reducing the electric potential gained from the electrochemical reactions. The geometry and/or materials of the SOFC could then be changed to reduce the losses. The "unit cell" can provide results which can improve and aid the design of solid oxide electrochemical cells.

The unit cell model can also be used to determine "equivalent" electrical and thermal conductivities for use in a model describing the operation of an SOFC stack. An SOFC stack is a collection of a large number of individual electrochemical cells connected in some appropriate manner (series or parallel with respect to current and/or reactant flows) to produce a usable quantity of power output. The equivalent conductivities are determined by comparing the flux of current and heat at the boundaries of the unit cell to the flux of current and heat computed with the stack model incorporating equivalent conductivities. Thus the unit cell provides a bridge between small scale modelling and macroscopic stack modelling.

References

- [1] Herbin, R., "Determination of Equivalent Conductivities for the Numerical Simulation of Solid Oxide Fuel Cells", report to the Swiss Federal Office of Energy, in preparation, 1991.
- [2] Appleby, A.J. and F.R. Foulkes, **Fuel Cell Handbook**, Van Nostrand Reinhold, New York, 1989.
- [3] Bossel, U.G. and J.R. Ferguson, "Natural gas fuelled solid oxide fuel cells & systems, facts & figures" IEA Workshop on Mathematical Modelling, Chermey, Switzerland, Ed.: Swiss Federal Office of Energy, 1989
- [4] Ferguson, J.R. "Analysis of temperature and current distributions in planar SOFC designs," Second Int. Symposium on Solid Oxide Fuel Cells, July 2-5, Athens, Greece, 1991.

Appendix

In section 5.3 the development of the electrical potential from the conservation of current principle showed the advantage of transforming the governing equation into a stream function formulation. The simplification of the boundary condition from a discontinuous jump of potential into a continuous variation of current across the boundary is noteworthy. As a consequence it is convenient to solve the entire "unit cell" electrical problem in terms of the stream function. The formulation of the stream function for the other computational domains is given here.

The geometry for the stream function formulation is shown in Fig. A1. The "unit cell" is divided into 3 regions, the oxidant side interconnect plus cathode (\equiv Region 1), the electrolyte (\equiv Region 2) and the fuel side interconnect plus anode (\equiv Region 3). In each of these domains, the governing equation describing the flow of current is

$$\frac{\partial}{\partial x} \left[\sigma \frac{\partial \varphi}{\partial x} \right] + \frac{\partial}{\partial y} \left[\sigma \frac{\partial \varphi}{\partial y} \right] = 0 \quad (\text{A1})$$

as developed from Eqs. 25, 37 and 38. The electrical conductivity, σ , is to be evaluated for the local material as appropriate.

Recalling the definition and properties of the stream function, the specification of boundary conditions is a straightforward procedure. Along boundary S_1 in each of the three regions the stream function is given a value of zero while along S_3 the stream function equals the total current flowing through the cell. Boundary S_5 in Regions 1 and 3 is merely an extension of boundary S_1 and therefore the stream function equals zero along this boundary as well. Along boundary S_2 of Region 1 and boundary S_4 of Region 3 the stream function is given a periodic condition since the "unit cell" is just one cell of a very large array of cells all of which behave in identical fashion. The boundary conditions at the interfaces between the three regions, the cathode-electrolyte-anode interfaces, were developed in Section 5.3. The boundary conditions can be summarized as:

Region 1: oxidant side interconnect plus cathode

$$\text{Boundary } S_1: \quad \varphi = 0 \quad (\text{A2})$$

$$\text{Boundary } S_2: \quad \frac{\partial \varphi}{\partial y} = \frac{\partial \varphi}{\partial y} \Big|_{S_4 \text{ Region 3}} \quad (\text{A3})$$

$$\text{Boundary } S_3: \quad \varphi = i_{\text{total}} \quad (\text{A4})$$

$$\text{Boundary } S_4: \quad \frac{\partial \varphi}{\partial y} = \frac{\partial \varphi_{el}}{\partial y} - \frac{RT}{8F} \frac{1}{p_{O_2}} \frac{\partial p_{O_2}}{\partial x} \quad (\text{A5})$$

$$\text{Boundary } S_5: \quad \varphi = 0 \quad (\text{A6})$$

Region 2: electrolyte

$$\text{Boundary } S_1: \quad \varphi = 0 \quad (\text{A7})$$

$$\text{Boundary } S_2: \quad \frac{\partial \varphi}{\partial y} = \frac{\partial \varphi_c}{\partial x} + \frac{RT}{8F} \frac{1}{p_{O_2}} \frac{\partial p_{O_2}}{\partial x} \quad (\text{A8})$$

$$\text{Boundary } S_3: \quad \varphi = i_{\text{total}} \quad (\text{A9})$$

$$\text{Boundary } S_4: \quad \frac{\partial \varphi}{\partial y} = \frac{\partial \varphi_a}{\partial x} + \frac{RT}{4F} \left[\frac{1}{p_{H_2O}} \frac{\partial p_{H_2O}}{\partial x} - \frac{1}{p_{H_2}} \frac{\partial p_{H_2}}{\partial x} \right] \quad (\text{A10})$$

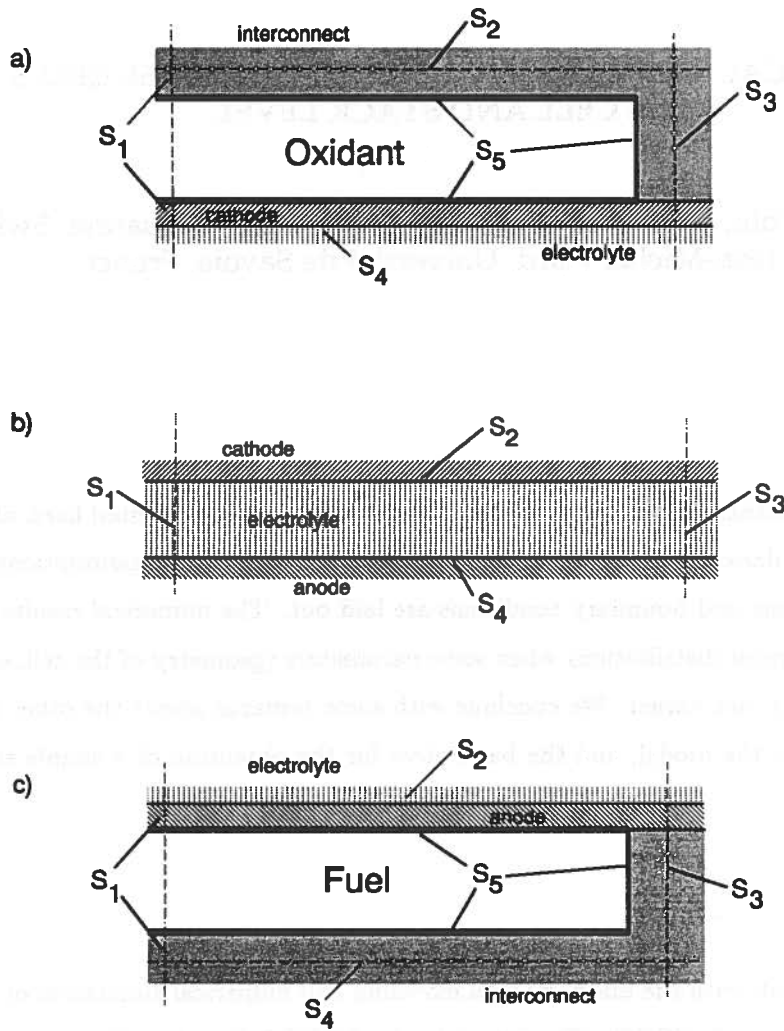


Figure A1. Computational for the stream function formulation: a) Region 1, b) Region 2 and c) Region 3.

Region 3: fuel side interconnect plus anode

$$\text{Boundary } S_1: \quad \varphi = 0 \quad (\text{A11})$$

$$\text{Boundary } S_2: \quad \frac{\partial \varphi}{\partial y} = \frac{\partial \varphi_{el}}{\partial y} - \frac{RT}{4F} \left[\frac{1}{p_{H_2O}} \frac{\partial p_{H_2O}}{\partial x} - \frac{1}{p_{H_2}} \frac{\partial p_{H_2}}{\partial x} \right] \quad (\text{A12})$$

$$\text{Boundary } S_3: \quad \varphi = i_{total} \quad (\text{A13})$$

$$\text{Boundary } S_4: \quad \frac{\partial \varphi}{\partial y} = \frac{\partial \varphi}{\partial y} \Big|_{S_2 \text{ Region 1}} \quad (\text{A14})$$

$$\text{Boundary } S_5: \quad \varphi = 0 \quad (\text{A15})$$

NUMERICAL SIMULATION OF SOLID OXIDE FUEL CELLS AT THE CELL AND STACK LEVEL.

Raphaèle Herbin, Ecole Polytechnique Fédérale de Lausanne, Switzerland.
Jean-Michel Fiard, Université de Savoie, France.

Abstract A 2D mathematical model of a Solid Oxide Fuel Cell is presented here, along with the results obtained by numerical simulation. The physics of the cell and the simplifying assumptions are first presented. Then the governing equations and boundary conditions are laid out. The numerical results show the behaviour of the temperatures and current distributions when some parameters (geometry of the cell, electrolyte materials, temperature in the channels) are varied. We conclude with some remarks about the other physical phenomena which we want to include in the model, and the basic ideas for the obtention of a simple stack model from the unit cell model.

1 Introduction

The work presented here deals with the mathematical modeling and numerical simulation of natural gas-fed solid oxide cells (Solid Oxide Fuel Cell, SOFC). The principle of a SOFC is based on the conversion of the chemical energy which is stored in the fuel (hydrogen or methane) into electrical energy through an electron-producing electrochemical reaction. The electrical energy produced by an electrochemical reaction depends on the reacting species concentrations through the Nernst law. A schematic diagram of the cell geometry is given in Figure 1, along with the main physical and chemical occurring processes, the list of which is the following :

1. The oxygen diffuses through the porous cathode material.
2. The oxygen molecules are dissociated and ionized at the cathode/electrolyte interface.
3. The oxygen ions migrate through the electrolyte towards the anode/electrolyte interface.
4. Hydrogen diffuses through the porous anode material.
5. Hydrogen reacts with the oxygen ions, producing water and liberating electrons, which flow back to the cathode/electrolyte interface.

The SOFC's systems seem to be of great interest for use of natural gas, because of their high power generation and heat recovery efficiency, as well as their low pollution rate. However, the ideal efficiency rate is never attained in experimental conditions. The most important losses are internal ohmic losses; diffusion losses and

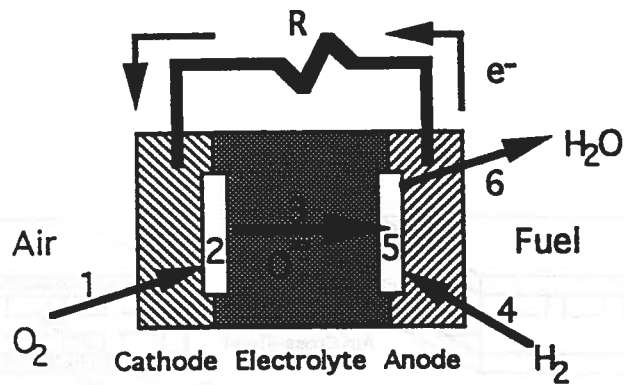


Figure 1

overpotential due to the electrochemical reactions can also be expected, even though they are usually thought to be less important than the ohmic losses. The aim of the mathematical modeling and numerical simulation of such a system is to give, for a given set of data describing the geometry of the cell and the operating conditions, an estimate of these losses and where they occur. Also, by varying the set of input parameters describing either the geometry or the operating conditions, the influence of these parameters on the efficiency of the cell can be studied. Numerical simulation of SOFCs has already been performed with mathematical models which were obtained with some simplifying assumptions (see [F] and references therein). The novelty here is that the temperature and current distributions are obtained within the unit cell itself, whereas in previous works, the solid material were assumed to be all at the same temperature and the current density was computed by averaging the conductivities of the various components. The mathematical model which is used here is the result of a collaboration with J.R. Ferguson and J.R. Selman (see [F] and [HS]).

2 A 2D mathematical model of a unit cell

2.1 Description of the geometry

The SOFC system is in fact a stack of electrochemical cells, i.e. it is made up of several repeating "unit cells". The lay out of the mathematical equations describing the physical and chemical phenomena can be carried out on the smallest non-repeating geometrical pattern which represents the unit cell. A planar bi-polar geometry is first studied, and, in order to obtain a 2D model, the cases of study are restricted here to co-flow and counter-flow (the cross-flow case yielding automatically a 3D model, see Figure 2, and, for instance [HS]); note that the results of [F] indicate that the co-flow geometry should be the most efficient. Here, in order to obtain a 2D model, all variables (temperature, electrical potential, concentrations of species) are assumed to be constant in the flow direction. The unit cell mathematical model has to be formulated before carrying out the numerical computations which will yield the behaviour of the physical entities for one unit cell. It can also be used to compute the same physical entities for a whole stack provided that the stack is made up of the same repeating unit cells, and that the boundary conditions at the channel walls are independent of the cells (i.e. same concentrations of species and same temperatures), with adequate boundary conditions on the exterior of the stack (thermal and electrical insulation). The planar bi-polar co- or counter-flow geometry which

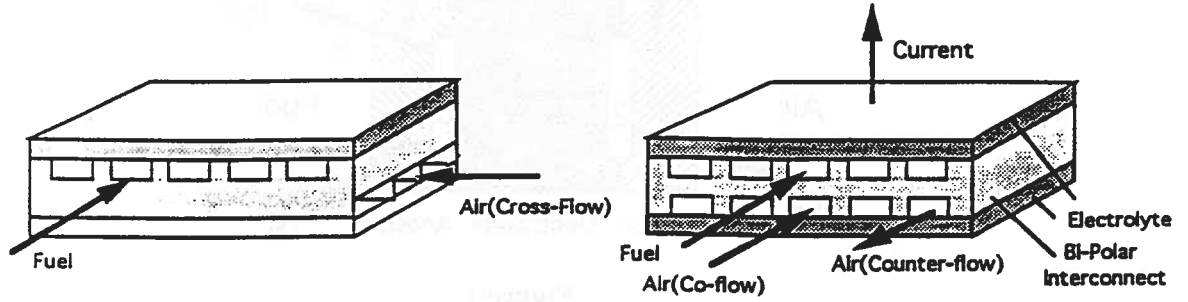


Figure 2

we consider here is depicted in Figure 3, and the geometrical parameters are defined. The cell is built around a PEN (Positive-Electrolyte-Negative) sandwich, where the electrochemical processes occur. The interconnect material supports the structure and also serves as the current collector. It is assumed to be made of a non-porous material. Hence the diffusion of oxygen only takes place through the cathode C and the diffusion of hydrogen (which is the fuel) takes place through the anode A .

2.2 The mathematical model

A 2D model is obtained by combining the conservation laws for heat, electrical current and mass with Fourier's law of heat conduction, Ohm's law, and Fick's law of diffusion, and writing the interface and boundary conditions. Let Φ denote the electrical potential, T the temperature, x_i the molar concentration of species i ($i = O_2, H_2, H_2O$). Then Φ , T and x_i satisfy the following equations :

$$-\text{div}(\sigma(T)\text{grad}\Phi) = 0 \text{ in } I, C, E \text{ and } A \quad (1)$$

$$-\text{div}(\lambda\text{grad}T) = \sigma(T)\text{grad}\Phi \cdot \text{grad}\Phi \text{ in } I, C, E \text{ and } A \quad (2)$$

$$-\text{div}\left(\frac{1}{1-x_{O_2}}\text{grad}x_{O_2}\right) = 0 \text{ in } C, \quad (3)$$

$$-\text{div}(\text{grad}x_{H_2}) = 0 \text{ in } A, \quad (4)$$

where $\sigma(T)$ is the (temperature dependent) electronic or ionic conductivity (depending on the region considered), and λ the thermal conductivity, $\text{grad}f$ denotes the gradient of a scalar function f : $\text{grad}f = \left(\frac{\partial f}{\partial x}, \frac{\partial f}{\partial y}\right)$, and $\text{div}g$ denotes the divergence of a vector function $g = (g_1, g_2)^T$: $\text{div}g = \frac{\partial g_1}{\partial x} + \frac{\partial g_2}{\partial y}$

The temperature is continuous throughout the solid material, in particular at all interfaces. The other interface conditions are now stated :

- C/I and A/I : cathode/interconnect and anode/interconnect interfaces
 - The heat flux $-\lambda\text{grad}T \cdot \mathbf{n}$ where \mathbf{n} denotes a normal to the interface, and the electrical current $-\sigma(T)\text{grad}\Phi \cdot \mathbf{n}$ are continuous
 - The electrical potential Φ is continuous.
- C/E : cathode/electrolyte interface

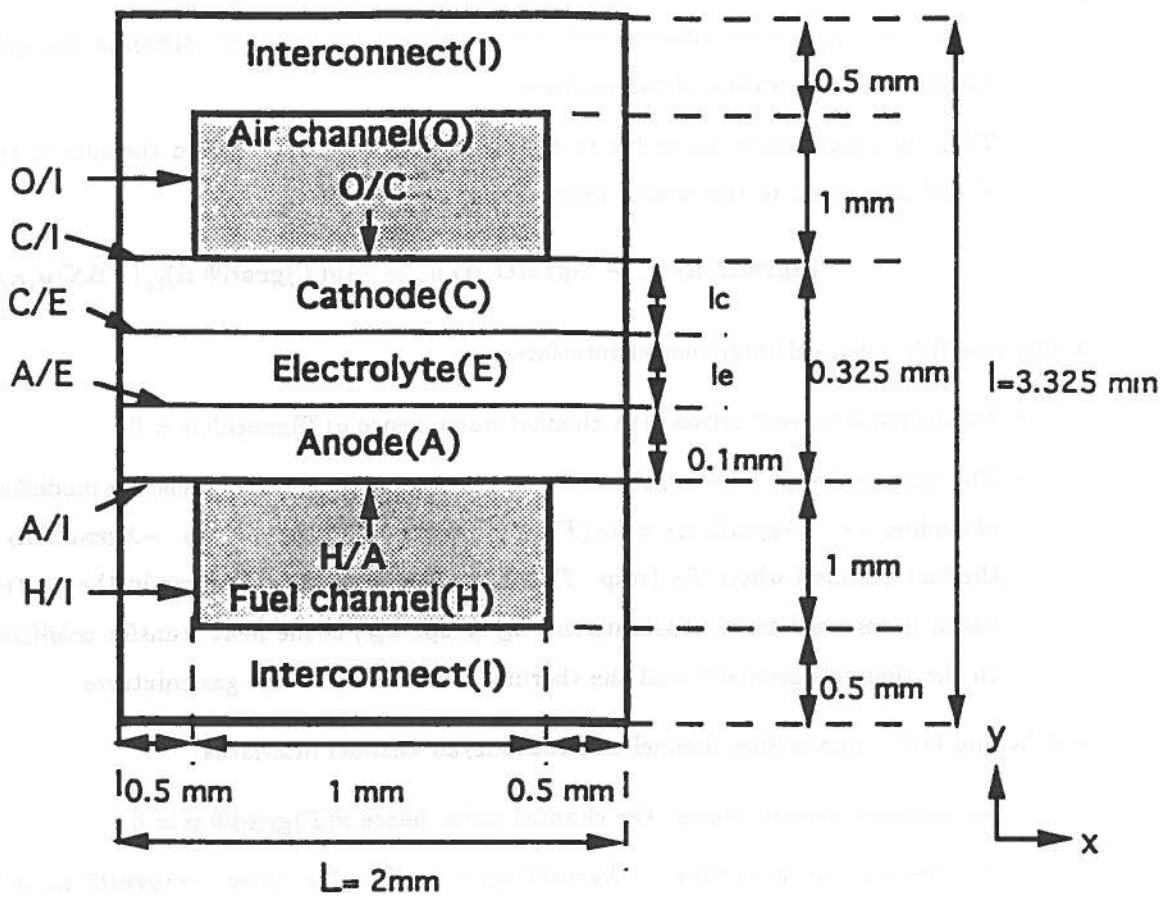


Figure 3

- The heat flux $-\lambda \text{grad} T \cdot \mathbf{n}$ where \mathbf{n} denotes a normal to the interface, and the electrical current $-\sigma(T) \text{grad} \Phi \cdot \mathbf{n}$ are continuous.
- There is a jump of potential at the cathode/electrolyte interface, equal to the value Φ_C^N of the Nernst potential of the chemical reaction $\frac{1}{2} O_2 + 2e^- \rightarrow O^{2-}$, hence : $\Phi_{|E} - \Phi_{|C} = \Phi_C^N$.
- The oxygen flux on the cathode side is related to the electrical current on the electrolyte side (i.e. the ion flux) by the relationship :

$$4Fc \left(\frac{D_{O_2-N_2}}{1-x_{O_2}} \text{grad} x_{O_2} \cdot \mathbf{n}_C \right)_{|C} = \left(\sigma(T) \text{grad} \Phi \cdot \mathbf{n}_E \right)_{|E}$$

where $D_{O_2-N_2}$ is the effective diffusion coefficient for oxygen diffusing through the cathode, c the molar concentration of the mixture, and \mathbf{n}_X denotes the normal to the boundary of domain X , outward to X .

• A/E : anode/electrolyte interface

- The electrical current $-\sigma(T) \text{grad} \Phi \cdot \mathbf{n}$ is continuous.
- There is a jump of potential at the anode/electrolyte interface, equal to the value Φ_A^N of the Nernst potential of the chemical reaction $H_2 + O^- \rightarrow H_2 + 2e^-$, hence : $\Phi_{|A} - \Phi_{|E} = \Phi_A^N$.
- The hydrogen flux on the anode side is related to the electrical current on the electrolyte side (i.e. the ion flux) by the relationship :

$$2F \left(c \frac{D_{H_2-H_2O}}{1-x_{H_2}} \text{grad} x_{H_2} \cdot \mathbf{n}_A \right)_{|A} = - \left(\sigma(T) \text{grad} \Phi \cdot \mathbf{n}_E \right)_{|E}$$

where $D_{H_2-H_2O}$ is the effective diffusion coefficient for hydrogen diffusing through the anode, and c the molar concentration of the mixture.

- There is a heat source term due to the same chemical reaction, and the sum of the heat fluxes from E and A is equal to this source term. Hence :

$$(\lambda \text{grad} T \cdot \mathbf{n}_E)|_E + (\lambda \text{grad} T \cdot \mathbf{n}_A)|_A = -(\sigma(T) \text{grad} \Phi \cdot \mathbf{n})|_A (T \Delta S)_{H_2O} / 2F.$$

- O/I and H/I : channel/interconnect interfaces

- No electrical current crosses the channel walls, hence $\sigma(T) \text{grad} \Phi \cdot \mathbf{n} = 0$.
- The heat exchange between the solid materials and the gas channels are modelled by Newton's law of cooling, i.e. $-\lambda \text{grad} T \cdot \mathbf{n}_I = h_O(T - T_O)$ for the air channel (resp. $-\lambda \text{grad} T \cdot \mathbf{n}_I = h_H(T - T_H)$ for the fuel channel) where T_O (resp. T_H) is the temperature of the gas in the air (resp. fuel) channel, which is assumed to be constant, and h_O (resp. h_H) is the heat transfer coefficient, which depends on the channels geometry and the thermal conductivity of the gas mixtures.

- H/A and O/C : anode/fuel channel and cathode/air channel interfaces

- No electrical current crosses the channel walls, hence $\sigma(T) \text{grad} \Phi \cdot \mathbf{n} = 0$.
- By Newton's law of cooling : $-\lambda \text{grad} T \cdot \mathbf{n}_A = h_H(T - T_H)$ (resp. $-\lambda \text{grad} T \cdot \mathbf{n}_A = h_O(T - T_O)$).
- The concentration of hydrogen at H/A is given by the concentration in the fuel channel : $x_{H_2} = (x_{H_2})_{\text{fuel}}$, and the concentration of oxygen is given by the concentration in the air channel : $x_{O_2} = (x_{O_2})_{\text{air}}$.

Before going to a numerical simulation, there remains to state the boundary conditions on Φ , T and x_i (and, if needed, on their gradients) on the external boundary of the cell. These boundary conditions depend on the operating conditions. The boundary conditions which are considered here are based on the idea that the cell is part of a whole stack, and they are stated in the following section, after transformation of the equations by the so-called "stream function" formulation.

2.3 Mathematical and numerical solution procedure

The interface conditions at C/E and C/A cannot be used as they are, because the partial Nernst potentials Φ_A^N and Φ_C^N are unknown separately; under simplifying assumptions, the sum $\Phi_A^N + \Phi_C^N$ can be shown to be equal to Φ^N , the Nernst potential of the overall reaction $H_2 + 1/2O_2 \rightarrow H_2O$. Following the idea of [F], a "stream function" formulation is introduced in order to circumvent this problem, i.e. the function $\psi(x, y)$ is defined by :

$$\frac{\partial \psi}{\partial x} = -\sigma \frac{\partial \Phi}{\partial y} \quad \frac{\partial \psi}{\partial y} = \sigma \frac{\partial \Phi}{\partial x}.$$

($\frac{\partial \psi}{\partial x}$ is therefore the electrical current in the y direction.) Hence, while the governing equations and boundary conditions for T and x_i remain unchanged, the equations in Φ are replaced by (see [FFH] for the details of this transformation) :

$$\text{div} \left(\frac{1}{\sigma} \text{grad} \psi \right) = 0$$

with the following boundary conditions :

$$\begin{aligned} \psi & \text{ is constant on the channel walls,} \\ \psi & \text{ and } \sigma \frac{\partial \psi}{\partial y} \text{ are continuous at } I/A \text{ and } C/I \\ \left(\frac{1}{\sigma} \frac{\partial \psi}{\partial y} \right)_{|E} - \left(\frac{1}{\sigma} \frac{\partial \psi}{\partial y} \right)_{|C} & = \frac{RT}{8F} \frac{\partial(\ln P_{O_2})}{\partial x} \text{ at } C/E \\ \left(\frac{1}{\sigma} \frac{\partial \psi}{\partial y} \right)_{|E} - \left(\frac{1}{\sigma} \frac{\partial \psi}{\partial y} \right)_{|A} & = \frac{RT}{4F} \left[\frac{\partial(\ln P_{H_2O})}{\partial x} - \frac{\partial(\ln P_{H_2})}{\partial x} \right] \text{ at } A/E \end{aligned}$$

The last two interface conditions are now possible to implement. Unfortunately, the stream function formulation does not extend easily to the 3D case. The external boundary conditions are taken to be :

$$\begin{aligned} \psi & = I_{avg}/2 \text{ at } x = 0, \text{ where } I_{avg} \text{ is the specified total current,} \\ \psi & = -I_{avg}/2 \text{ at } x = L, \\ \psi(x, 0) & = \psi(x, l) \text{ and } \frac{\partial \psi}{\partial y}(x, 0) = \frac{\partial \psi}{\partial y}(x, l). \end{aligned}$$

Now that an apparently well-posed mathematical problem has been obtained, the next necessary step in order to perform a numerical simulation is to discretize the set of equations in T , Φ and x_i . The equations themselves are of the Laplacian type and can be successfully discretized by any of the usual methods, i.e. finite differences, finite element or finite volumes. However, because of the presence of interface sources, the finite volume discretization has been preferred (see [P], [FGH] for an introduction). Indeed, the main advantage of the finite volume method is that it is "close to the physics" in the sense that it is based on writing the balance of the fluxes through the boundaries of a discretization cell (which is called a "control volume"), and therefore all source terms can be accounted for in a natural way. The discretization of the equations (see [FFH] for details) yield a nonlinear finite system, where the unknowns are the average values (over the control volumes) of T , ψ and x_i . The equations in T , ψ , x_i are coupled by the electrical conductivity (which depends on the temperature), the ohmic source terms and the interface source terms, both in T and ψ . A rather straightforward iterative method is used, which computes, for a given temperature, the solution to the mass and electric problems (x_i and ψ), and once convergence is obtained, solves the temperature problem, as described in Figure 4.

3 Numerical results

The physical and chemical data which were used for the numerical simulation are presented here (section 3.1). Then a series of numerical tests are described, which yield some knowledge about the behaviour of the effective potential of the cell and the various losses. The series of runs which are presented were performed with the following variations of the parameters :

- cell geometry (section 3.2).
- diffusion coefficients (section 3.3).
- temperature of hydrogen in the channel (section 3.4).
- molar fraction of hydrogen in the channel (section 3.5).
- electrolyte material (section 3.6).

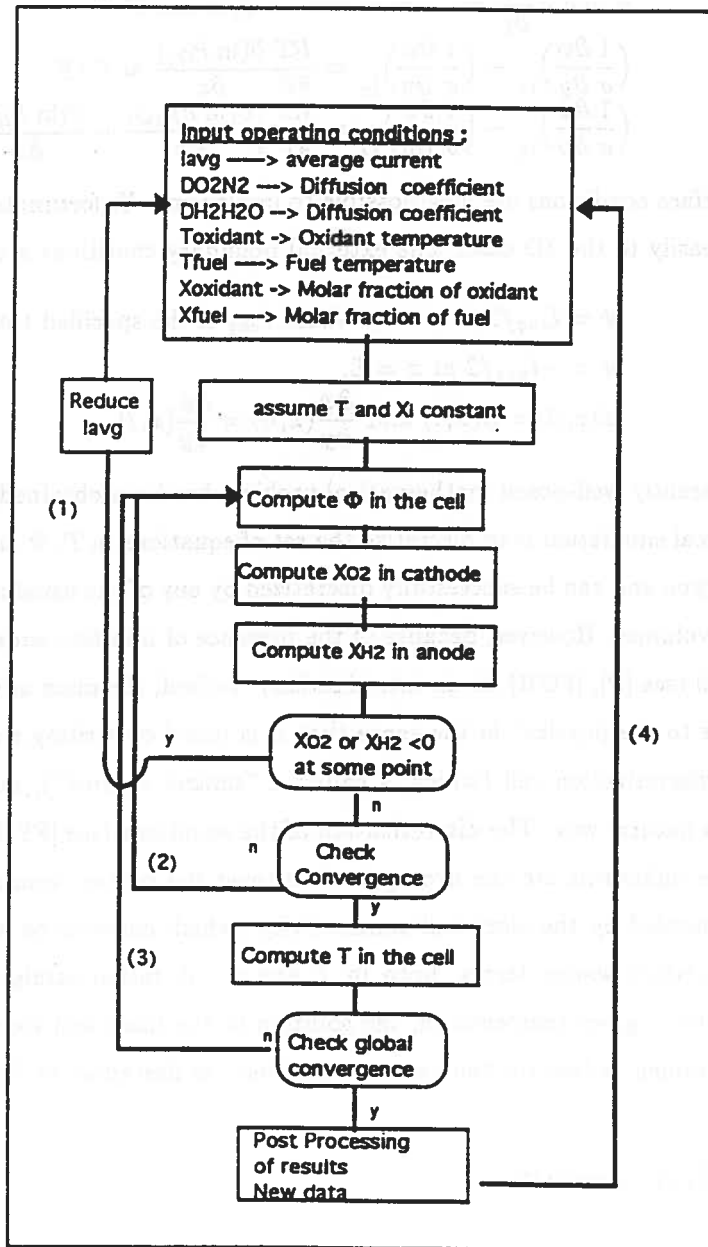


Figure 4

Code	Scientific name	Function	Thermal conductivity	Electrical conductivity
			$WK^{-1}m^{-1}$	$\Omega^{-1}m^{-1}$
C1	Strontium doped lanthanum manganite	Cathode	3	12880
E1	Yttria stabilized zirconia	Electrolyte	2	6.252
E2	Yttria stabilized zirconia	Electrolyte	2	8.879
E3	Yttria and ytterbia stabilized zirconia	Electrolyte	2	11.97
A1	Nickel zirconia cermet	Anode	3	30360
I1	Strontium doped lanthanum chromite	Interconnect	3.5	3100
O2	Oxygen	Oxidant	0.0832 at 1200 K	
H2	Hydrogen	Fuel	0.4966 at 1200 K	

Table 1

Code	Unit	Scientific name	Range of values
I_{avg}	A/cm^2	Average current crossing the cell	{0, 4}
$D_{O_2-N_2}$	cm^2/s	Effective diffusion coefficient of O_2	{0.2, 1}
$D_{H_2-H_2O}$	cm^2/s	Effective diffusion coefficient of H_2	{1, 5}
T_{O_2}	K	Fluid bulk temperature of O_2	{1150, 1200}
T_{H_2}	K	Fluid bulk temperature of H_2	{1200}
X_{O_2}	no unit	Mole fraction of O_2 in channel	{0.2}
X_{H_2}	no unit	Mole fraction of H_2 in channel	{0.05, 0.85}

Table 2

3.1 Physical data

Geometry

The geometry of the cell which is considered here is as presented in Figure 3. A discretisation mesh of 440 control volumes was used. The varying parameters in the numerical tests are the thickness of the electrolyte (l_e varies from .025 mm and .05 mm) and the thickness of the cathode (l_c varies from .175 mm and .2 mm), while the total thickness of the PEN remains constant (all data are shown on Figure 3).

Materials and gas mixtures

The materials and the gas mixtures are shown in Table 1, and were recommended in [BF] (fuel is considered to be hydrogen).

Other data The other relevant data which were used in the numerical simulations are presented in Table 1 for those which are varied for different runs and in Table 2 for the data which remain constant throughout the runs.

3.2 Influence of the geometry of the PEN

Parameters	Values or Codes
Cathode	C1
Anode	A1
Interconnect	I1
Oxidant	O2
Fuel	H2
T_{H_2} (K)	1200
X_{O_2}	0.2

Table 3

Fixed Parameters	Values or Codes
Electrolyte	E1
T_{O_2} (K)	1200
X_{H_2}	0.2
$D_{O_2-N_2}$ (cm^2/s)	0.2
$D_{H_2-H_2O}$ (cm^2/s)	1
Variable Parameters	Range of Values
l_c (mm)	{0.175, 0.200}
l_e (mm)	{0.025, 0.050}
I_{avg} (A/cm^2)	{0, 4}

Table 4

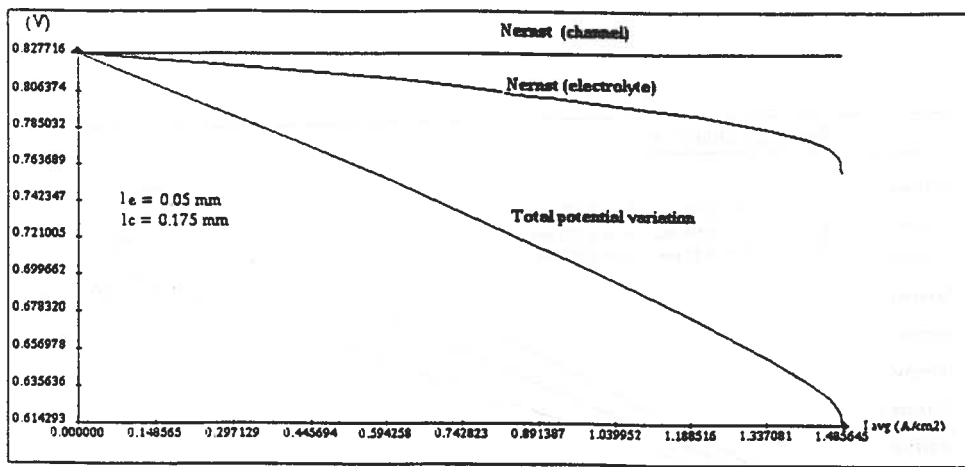


Figure 5

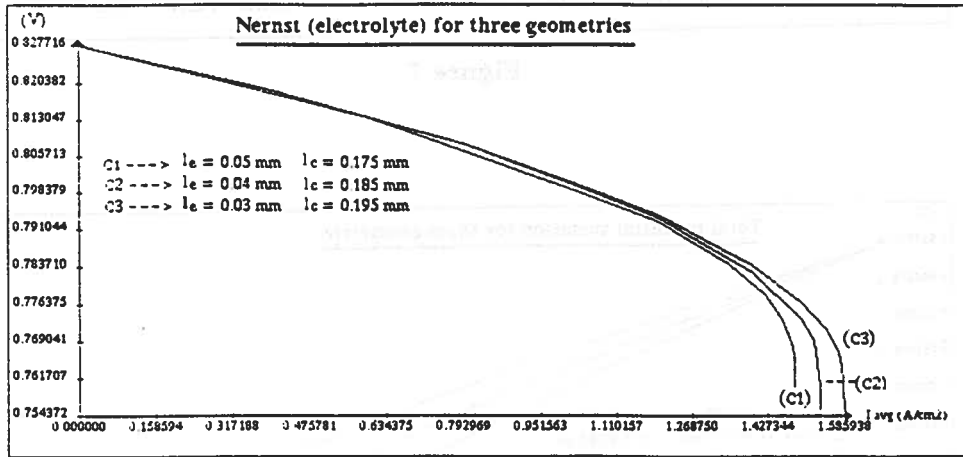


Figure 6

The data which were used for this series of run are summarized in Table 4. Note that the cathode thickness and the electrolyte thickness vary, while the anode thickness and the overall PEN thickness remain constant. Three different geometries were studied. The diagram of Figure 5 shows, for the first case of Table 4, the behaviour of the Nernst potential computed at the electrolyte and the total potential variation. All potentials are in fact computed by averaging the exact potential along the considered interface. The difference between the Nernst computed at the channel and the Nernst computed at the electrolyte represents the potential loss by diffusion, while the difference between the Nernst at electrolyte and the total potential variation represents the ohmic loss. The diagram of Figure 6 shows the influence of the geometry of the PEN on the Nernst potential. Notice that the Nernst potential decreases with the the electrolyte thickness decreases. Figure 7 shows the influence of the PEN geometry on the ohmic part of the potential loss. It can noted that the ohmic loss decreases with the electrolyte thickness. This is due to the fact that the electrolyte conductivity is much smaller than the other materials conductivities, so that the resistance in the cell is primarily due to the electrolyte. Figure 8 shows the influence of the PEN geometry on the total potential loss (i.e. diffusion + ohmic).

3.3 Influence of the diffusion coefficients

The data which were used for this series of run are summarized in Table 5.

For small values of the diffusion coefficients, the total (average) electrical current that is imposed on the cell is

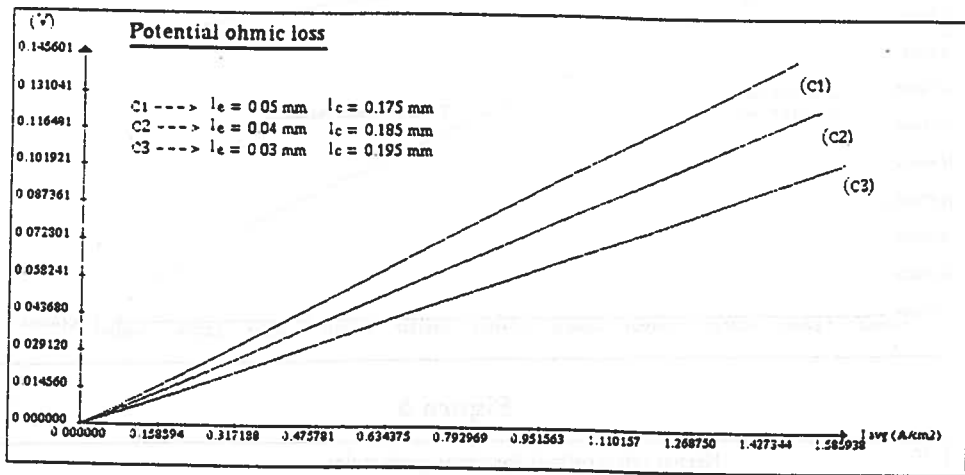


Figure 7

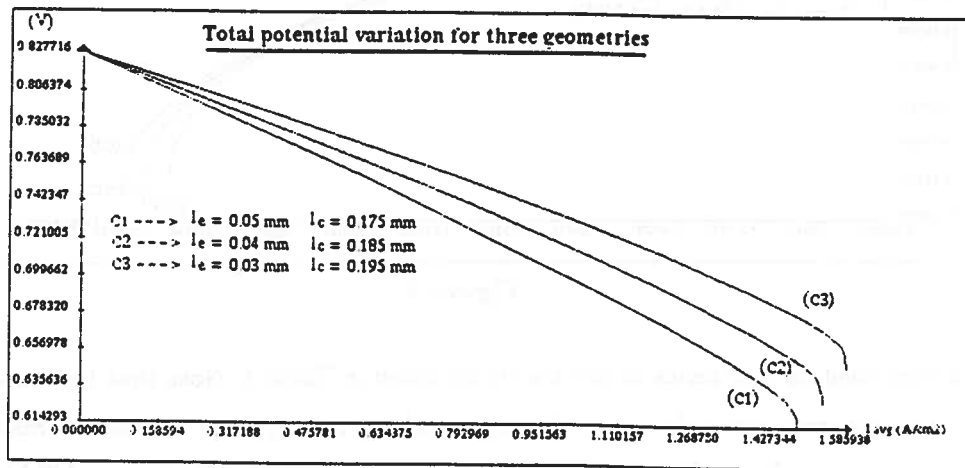


Figure 8

Fixed Parameters	Values or Codes
Electrolyte	E1
l_e (mm)	0.175
l_c (mm)	0.050
T_{O_2} (K)	1200
X_{H_2}	0.2
Variable Parameters	Range of Values
$D_{O_2-N_2}$ (cm^2/s)	{0.2, 1}
$D_{H_2-H_2O}$ (cm^2/s)	{1, 5}
I_{avg} (A/cm^2)	{0, 4}

Table 5

	$D_{O_2-N_2} = 0.2$	$D_{O_2-N_2} = 0.466$	$D_{O_2-N_2} = 0.773$	$D_{O_2-N_2} = 1$
$D_{H_2-H_2O} = 1$	1.485742	2.220437	2.220437	2.220437
$D_{H_2-H_2O} = 2.33$	1.485742	3.466518	> 4	> 4
$D_{H_2-H_2O} = 3.66$	1.485742	3.466518	> 4	> 4
$D_{H_2-H_2O} = 5$	1.485742	3.466518	> 4	> 4

Table 6

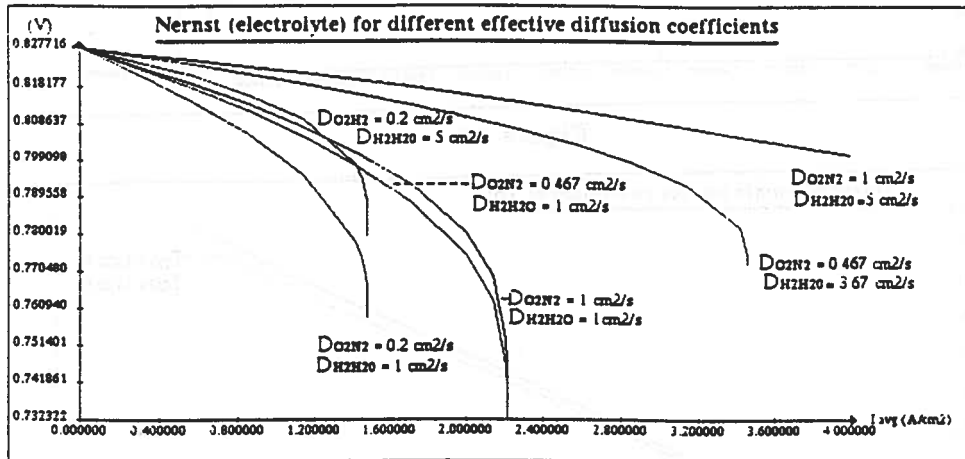


Figure 9

limited by the fact that the potential drops at a certain current, called "voltage drop current" ; this is due to the fact that the Nernst potential drops if the molar fraction of oxygen at the electrolyte/cathode interface (or of hydrogen at the electrolyte/anode interface). The limiting factor is therefore either $D_{O_2-N_2}$ or $D_{H_2-H_2O}$, depending on the values of these coefficients. These results are summarized in Table 6 and Figure 9.

3.4 Influence of the air temperature in the channel

The data which were used for this series of run are summarized in Table 7.

The Nernst potential is a function of the temperature and of the concentrations. When the temperature of the

Fixed Parameters	Values or Codes
Electrolyte	E1
le (mm)	0.175
lc (mm)	0.050
X_{H_2}	0.2
$D_{O_2-N_2}$ (cm^2/s)	0.2
$D_{H_2-H_2O}$ (cm^2/s)	1
Variable Parameters	Range of Values
T_{O_2} (K)	{1150, 1200}
I_{avg} (A/cm^2)	{0, 4}

Table 7

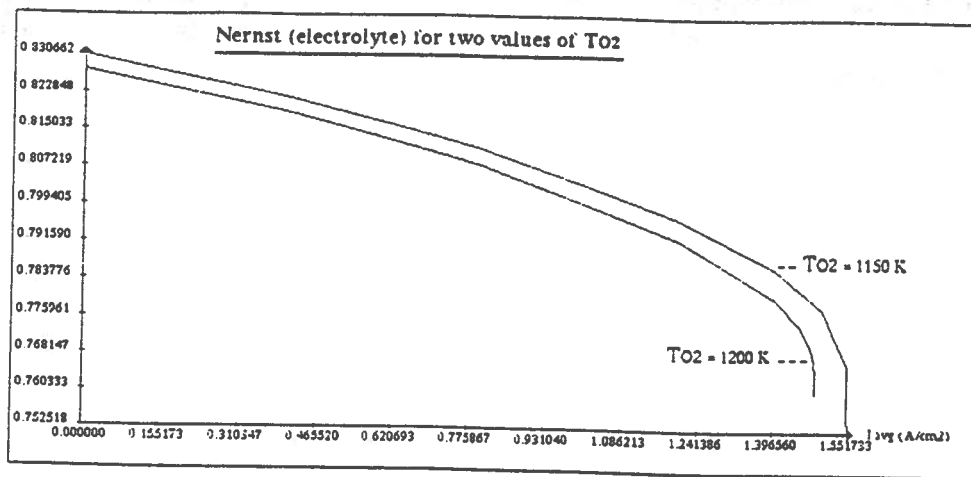


Figure 10

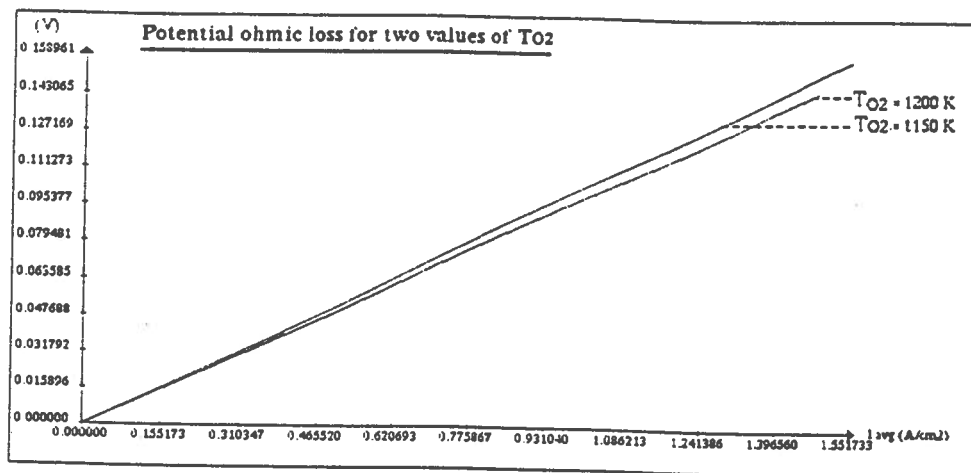


Figure 11

air in the air channel changes, this influences both the Gibbs free energy, which depends only on the temperature, and the concentrations at the interfaces (through the coupling of the various equations). The Nernst potentials for the two temperatures are displayed in Figure 10. The values of the Nernst potentials at $I_{avg} = 0$ is only due to the influence of the temperature on the Gibbs free energy. Figure 11 shows that the ohmic potential loss is greater when the air temperature decreases; this is due to the fact that the electrolyte conductivity decreases with the temperature. Figure 12 shows the total potential loss as a function of temperature. The potential loss does not vary much except at very low and very large currents.

3.5 Influence of the molar fraction of hydrogen in the channel

The data which were used for this series of run are summarized in Table 8.

Figure 13 (which displays the Nernst potential for various molar concentrations) shows that if x_{H_2} is large enough, the "potential drop current" does not depend on x_{H_2} anymore, but only on the value of the diffusion coefficients. The variation of x_{H_2} did not, however, affect the ohmic loss.

3.6 Influence of the electrolyte material

The data which were used for this series of run are summarized in Table 9.

Figures 14 and 15 show that the electrolyte material which is used does not influence the loss by diffusion, but

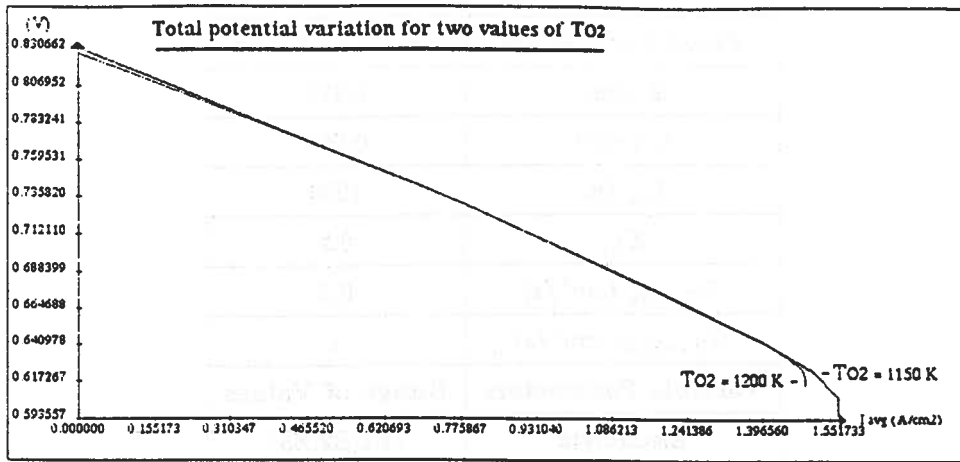


Figure 12

Fixed Parameters	Values or Codes
Electrolyte	E1
l_e (mm)	0.175
l_c (mm)	0.050
T_{O_2} (K)	1200
$D_{O_2-N_2}$ (cm^2/s)	0.2
$D_{H_2-H_2O}$ (cm^2/s)	1
Variable Parameters	Range of Values
X_{H_2}	{0.05, 0.85}
I_{avg} (A/cm^2)	{0, 4}

Table 8

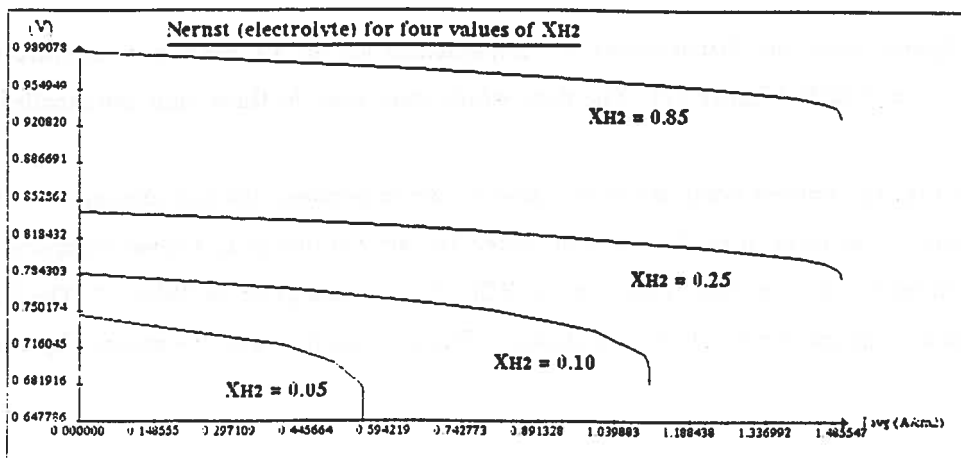


Figure 13

Fixed Parameters	Values or Codes
l_e (mm)	0.175
l_c (mm)	0.050
T_{O_2} (K)	1200
X_{H_2}	0.2
$D_{O_2-N_2}$ (cm^2/s)	0.2
$D_{H_2-H_2O}$ (cm^2/s)	1
Variable Parameters	Range of Values
Electrolyte	{E1,E2,E3}
I_{avg} (A/cm^2)	{0, 4}

Table 9

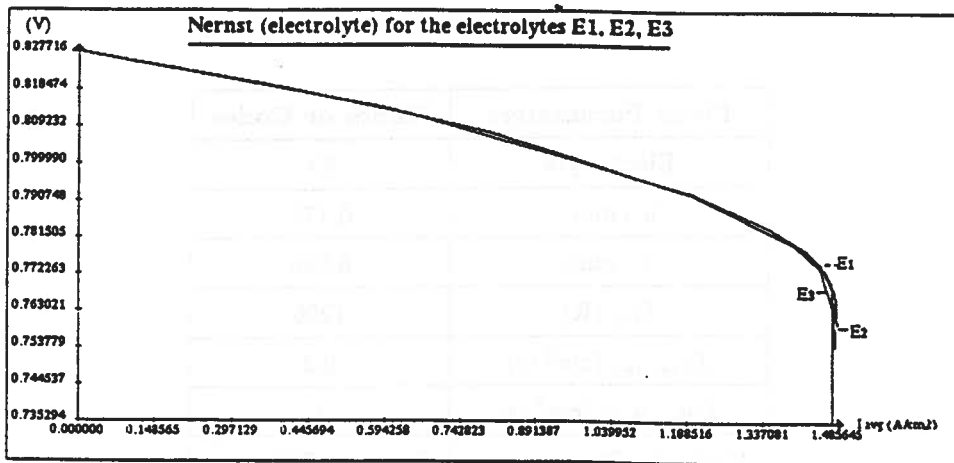


Figure 14

influences the ohmic loss. The best material seems to be E3; this is due to the fact that its ionic conductivity is the largest.

3.7 Distributions of electrical current and temperature

The following figures show the distributions of temperatures for an air channel temperature of $T = 1200K$ (Figure 16) and $T = 1150K$ (Figure 17). The data which were used for these runs are recalled in tables 10 and 11 respectively.

It can be noted that the hottest point of the cell moves from in between the two channels when these are at the same temperature to the sides of the fuel channel when the air channel is at a lower temperature.

The last figure shows the distribution current in the PEN, for the data given in Table 11. The largest currents are located in the anode, at the corner of the fuel channel. These could probably be reduced by using "rounded-off" corners.

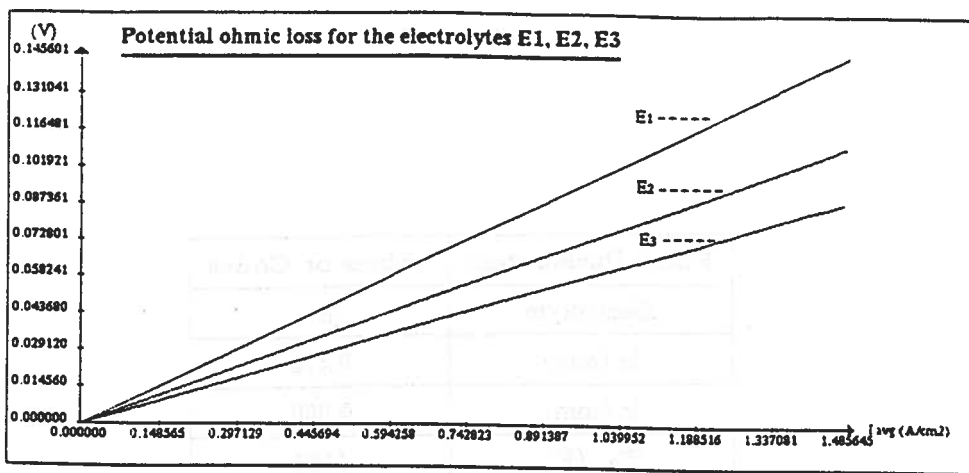


Figure 15

Fixed Parameters	Values or Codes
Electrolyte	E1
le (mm)	0.175
lc (mm)	0.050
T_{O_2} (K)	1200
X_{H_2}	0.2
$D_{O_2-N_2}$ (cm ² /s)	0.2
$D_{H_2-H_2O}$ (cm ² /s)	1
I_{avg} (A/cm ²)	1

Table 10

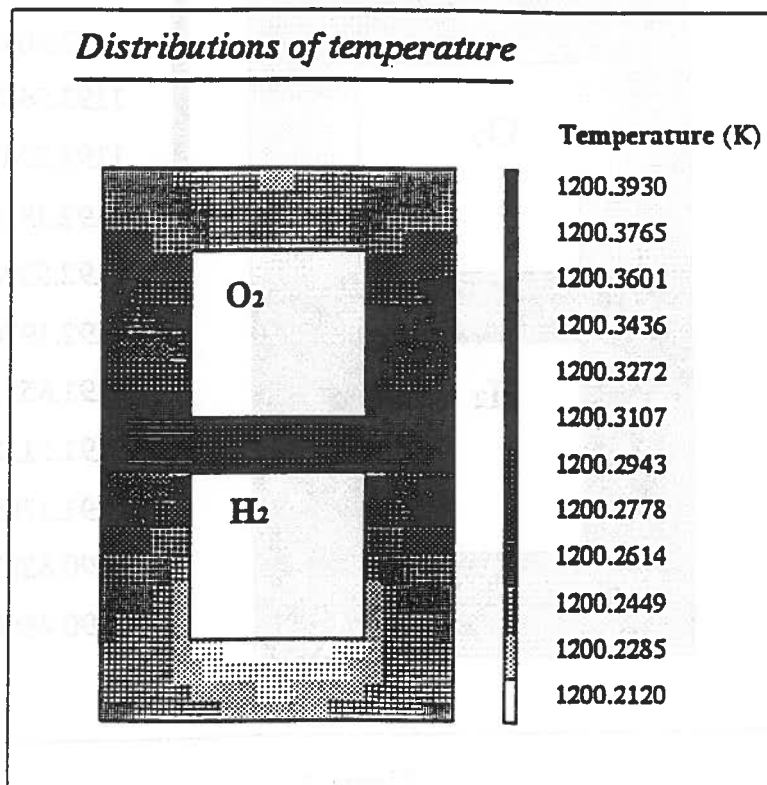


Figure 16

Fixed Parameters	Values or Codes
Electrolyte	E1
l_e (mm)	0.175
l_c (mm)	0.050
T_{O_2} (K)	1150
X_{H_2}	0.2
$D_{O_2-N_2}$ (cm^2/s)	0.2
$D_{H_2-H_2O}$ (cm^2/s)	1
I_{avg} (A/cm^2)	1

Table 11

Distributions of temperature

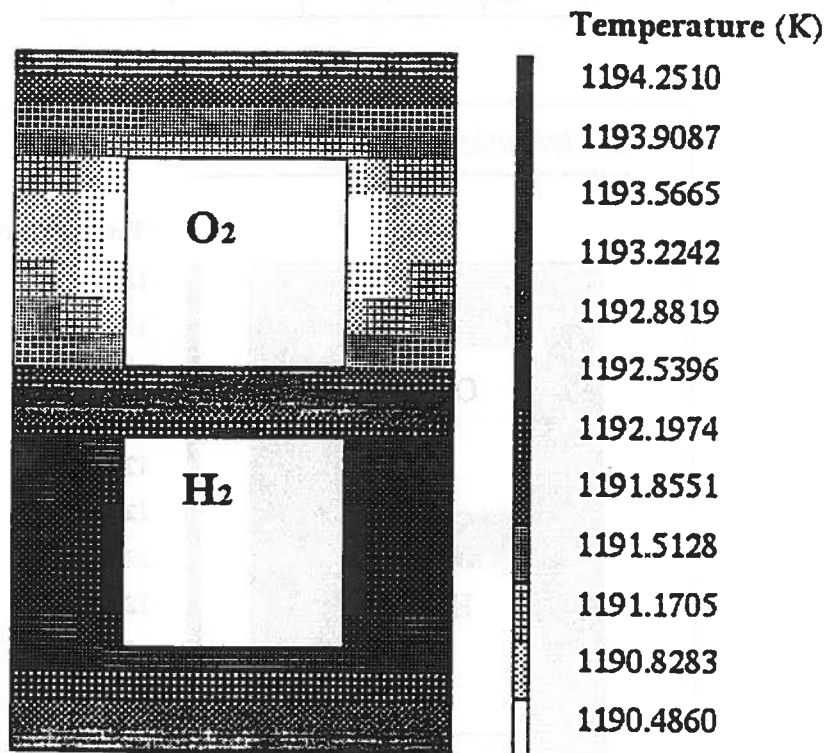


Figure 17

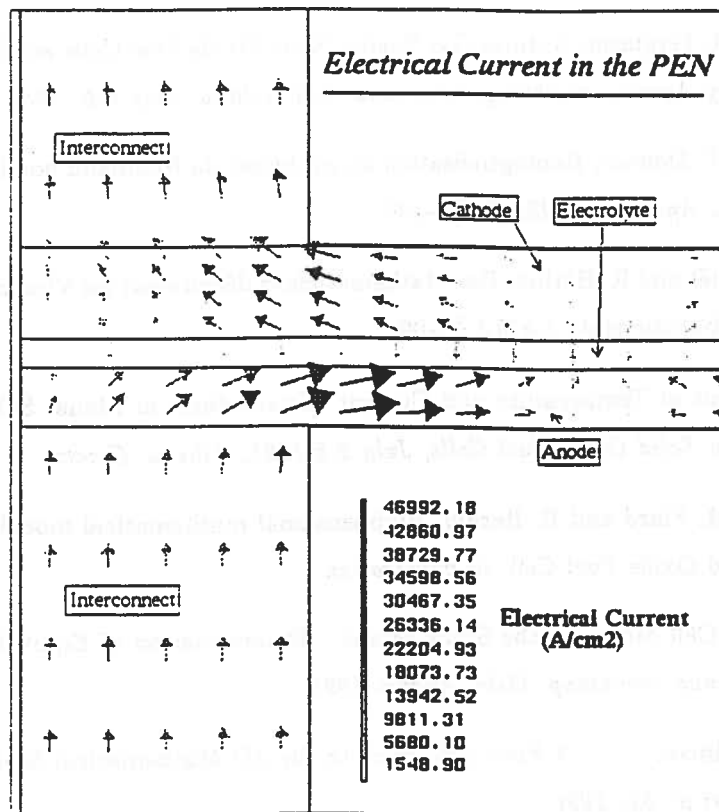


Figure 18

4 Conclusions

The numerical results which were obtained here give some interesting results concerning the efficiency of a SOFC w.r.t. its geometrical parameters and operating conditions. The next step will be to take the electrochemical overpotential into account. This amounts to adding another source term at the anode/electrolyte interface conditions. This term is nonlinear and will also be treated by the fixed point method. Another generalisation to be made is to consider the fuel to be methane, and take into account the reforming of the methane.

A stack model is also under study. Following the idea of [OS], since the stack is made up of a great number of cells, a model can be driven on a scale much larger than the scale of the cell (therefore, the number of cells is considered to be much larger than the number of control volumes). This stack model can be obtained from the cell model using ideas from homogenisation theory ([SP], [CD]), through the computation of "equivalent conductivities" [H].

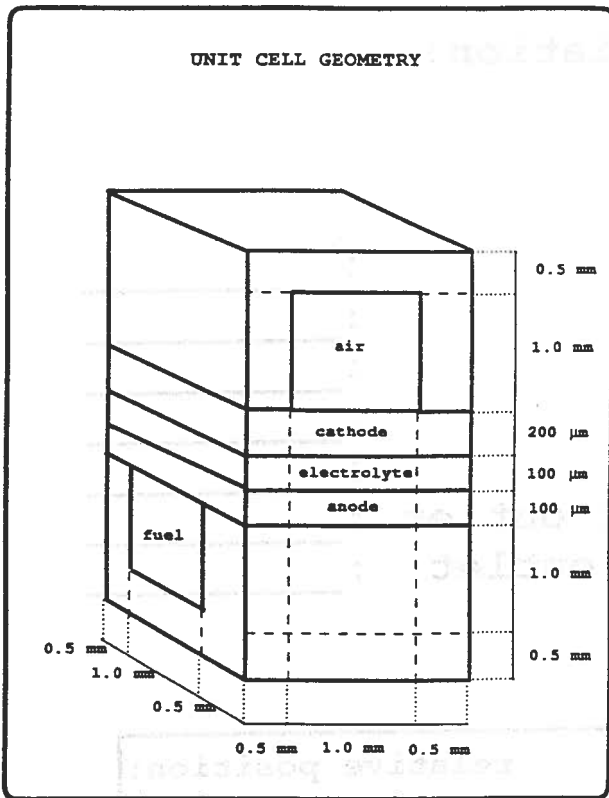
5 Acknowledgments.

The work of the authors was supported by Gaz de France for the first author and by OFEN (Switzerland) for the second author. The authors would also like to thank James Ferguson and Thierry Gallouët for numerous and fruitful discussions.

6 References.

- [BF] U.G. Bossel and J.R. Ferguson, Natural Gas Fuelled Solid Oxide Fuel Cells and Sytems, Facts and Figures, *International Energy Agency, workshop, Charmey, Switzerland, July 2-6, 1989.*
- [CD] D. Cioranescu and P. Donato, Homogénéisation du problème de Neumann non homogène dans des ouverts perforés, *Asymptotic Analysis 1 (1988) 115-138.*
- [FGH] I. Faille, T. Gallouët and R. Herbin, Des Mathématiciens découvrent les Vloumes Finis, *Matapli October 1991 and Les Prépublications du LAMA 91-09a.*
- [F] J.R. Ferguson, Analysis of Temperature and Current Distributions in Planar SOFC Designs, *2nd International Symposium on Solid Oxide Fuel Cells, July 2-5, 1991, Athens, Greece.*
- [FFH] J.R. Ferguson, J.M. Fiard and R. Herbin, Bidimensional mathematical modeling and numerical simulation of a planar Solid Oxide Fuel Cell, *in preparation.*
- [H] R. Herbin, From the Cell Model to the Stack Model : Determination of Equivalent Conductivities, *International Energy Agency, workshop, Oslo, August 1991.*
- [HS] R. Herbin and R.Selman, A First Approach to the 3D Mathematical Modeling of Solid Oxide Fuel Cells, *GASOV Report n° 34, 1990.*
- [OS] M. Ostenstad T. Sira, Numerical Modelling of SOFC, Design Proposal, *Institutt for Energiteknikk, N-1751, Halden, Norway.*
- [P] S.V. Patankar, Numerical Heat Transfer and Fluid Flow, *Series in Computational ethods in Mechanics and Thermal Sciences, Minkowycz and Sparrow Eds., Mc Graw Hill.*
- [SP] E. Sanchez-Palencia, Non-homogeneous Media and Vibration Theory, *Lecture Notes in Physics 127 (springer, Berlin, 1980).*

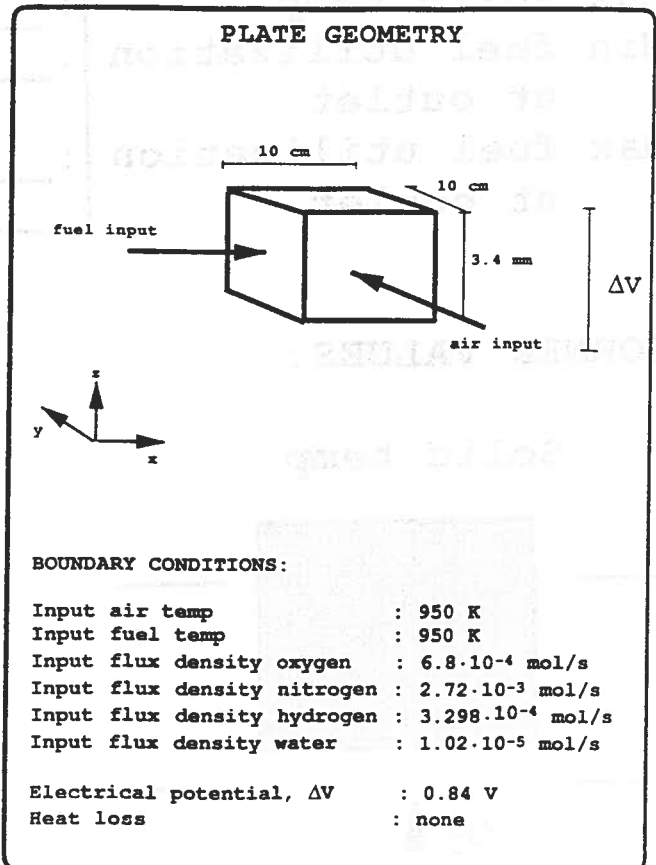
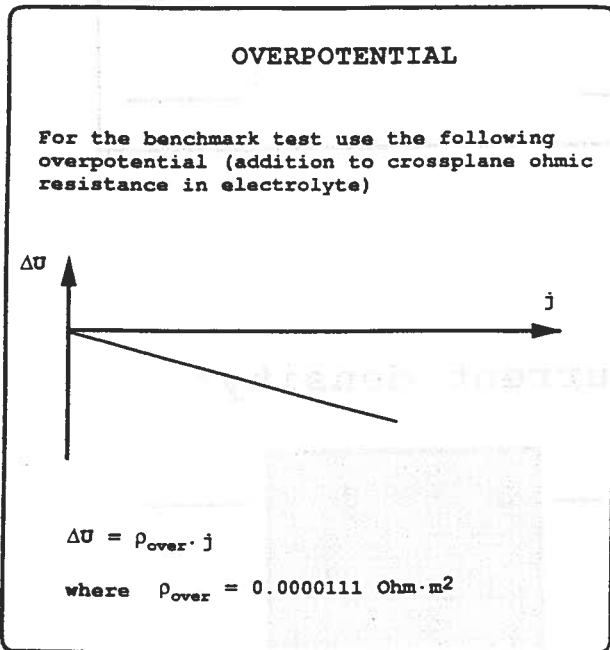
BENCHMARK CASE DEFINITION



MATERIAL DATA

For the benchmark test use the following values for thermal and electrical conductivities. (From Facts & Figures)

material	λ (W/m·K)	σ (ohm ⁻¹ m ⁻¹)
Electrolyte	2	$33400e^{-(10300/T)}$
Cathode	3	$42 \cdot 10^6/T \cdot e^{-(1200/T)}$
Anode	3	$95 \cdot 10^6/T \cdot e^{-(1150/T)}$
Interconnect	3.5	$9.3 \cdot 10^6/T \cdot e^{-(1100/T)}$



BENCHMARK REPORT

Model name:

Modeller:

Affiliation:

AVERAGE VALUES:

Solid temperature	:	_____
Current density	:	_____
Air temp at outlet	:	_____
Fuel temp at outlet	:	_____
Fuel utilization at outlet	:	_____
Solid temp minus fuel temp at outlet	:	_____
Solid temp minus air temp at outlet	:	_____

LOCAL VALUES:

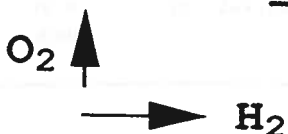
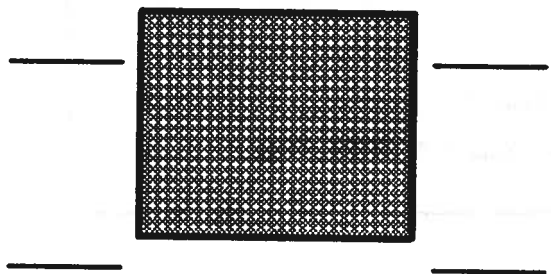
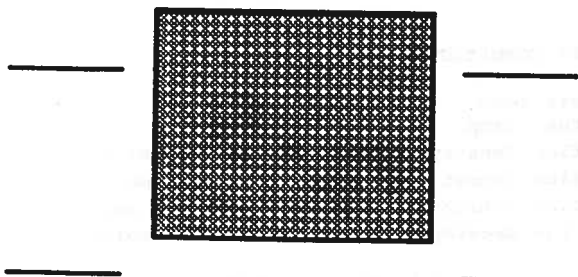
Min solid temp
 Max solid temp
 Min fuel utilization
 at outlet
 Max fuel utilization
 at outlet

value:	relative position:	
	x	y
: _____	: _____	: _____
: _____	: _____	: _____
: _____		: _____
: _____		: _____

CORNER VALUES:

Solid temp:

Current density:



Temperatures in Kelvin,
 Current densities in A/m²